OPTIMIZATION OF JET IMPINGEMENT CHANNEL FOR NEAR WALL COOLING IN GAS TURBINE AIRFOILS

by

Nicholas Ryan Miller

B.S. in Chemistry, Waynesburg University, 2009

Submitted to the Graduate Faculty of

the Swanson School of Engineering in partial fulfillment

of the requirements for the degree of

Master of Science in Mechanical Engineering

University of Pittsburgh

2013

UNIVERSITY OF PITTSBURGH

SWANSON SCHOOL OF ENGINEERING

This thesis was presented

by

Nicholas Ryan Miller

It was defended on

November 13, 2013

and approved by

Mark Kimber, Ph. D, Assistant Professor, Department of Mechanical Engineering and Materials Science

Qing-Ming Wang, Ph. D, Professor, Department of Mechanical Engineering and Materials Science

Thesis Advisor: Minking K. Chyu, Ph. D, Professor, Department of Mechanical Engineering and Materials Science

OPTIMIZATION OF JET IMPINGEMENT CHANNEL FOR NEAR WALL COOLING IN GAS TURBINE AIRFOILS

Nicholas R. Miller, M.S.

University of Pittsburgh, 2013

The current experimental study focuses on the heat transfer and pressure effects of a single array jet impingement channel. This study is broken down into three parts: 1) varying flow and varying diameters, 2) effects of jet configuration by staggering and angling jets, and 3) the effects of surface roughness on jet impingement. A single row of five jets, individually fed for the varying flow case and plenum fed for all other cases expels air onto the target surface as the spent air is constrained to exit in only one direction, causing jets to encounter maximum crossflow. The baseline jet plate parameters were defined as diameter, D, height to diameter H/D, and jet-to-jet spacing, S/D, are 9.53 mm (0.375 in), 2 and 4, respectively. The Reynolds Number, Re, for these studies ranged from 50,000 to 80,000. A transient liquid crystal technique is employed to determine the local and average heat transfer coefficient distribution on the target plate. Commercially available CFD software, ANSYS CFX, is used to correlate experimental results and to provide detailed insights of the flow field created by the array of jets. Additionally, two stainless steel coupons representing the jet impingement array at realistic size were tested and compared to results reported in literature.

By varying the jet flow rates by approximately ± 2% over the baseline case, local heat transfer enhancement on the target surface is increased up to 35%. Using the flow rates from the optimum varying flow case, a jet plate with varying diameters was created. Unfortunately, enhancement was not as significant in the varying diameter case due to the nature of flow distribution from the plenum.

Staggered jets, 1D and 2D, and staggered angled jets, 1D and 2D with 30° inclination were compared to the baseline case. Staggered jets, because of interactions with the channel side walls show no enhancement over the baseline. However, jets staggered 1D with 30° inclination show a heat transfer enhancement of $\approx 20\%$.

For the final part, surface roughness is explored. In general, different shaped ribs tend to enhance heat transfer by increasing the surface area of the target plate. As found in this study, and also reported in literature, horizontal ribs can cause entrainment, thus reducing the effectiveness of the jet impingement. If strategically placed, as for the X-shaped ribs, further enhancement can be achieved, especially in the downstream regions of the channel where crossflow tends to affect jet impingement.

TABLE OF CONTENTS

LIST OF TABLES

LIST OF FIGURES

NOMENCLATURE

Roman Letters

D	Jet diameter
D_h	Jet channel hydraulic diameter
e	Rib Height
f	Friction factor, $(\Delta P/\rho(U^2/2))(D_h/L)$
h	Heat transfer coefficient (W/m^2-K)
H	Jet channel height
k	Thermal conductivity of air
Nu	Nusselt number
p	Rib pitch
P	Pressure
Pr	Prandlt number
Re	Reynolds number, UD_h/ν
S	Jet-to-jet spacing (streamwise)
T	Temperature
U	Bulk mean velocity of jet channel

Greek symbols

ρ	Density

μ Viscosity

Superscript

◦ Degree

Subscript

0 Smooth channel

ACKNOWNLEDGEMENTS

I'd like to first thank the University of Pittsburgh's Swanson School of Engineering. The school gave a non-typical engineering student a chance to enter the program and succeed in a new field. In the same context, I'd like to thank my advisor Dr. Minking K. Chyu. He not only took a chance on me, but gave me free range in my decision making when it came to my work. His encouragement and teaching pushed me to new levels every day. Thanks are given to my committee members, Dr. Mark Kimber and Dr. Qing-Ming Wang, for volunteering their time and energy to this project. I'd also like to thank my mentor/colleague Dr. Sin Chien Siw for all the help and encouragement he gave me over the past 2 years.

As I have spent 4 years working (2 years as a contractor and 2 years under the RUA) at the National Energy Technology Lab under the direction of the Department of Energy, I have many people to thank. I'd like to thank Dr. Randall Gemman, Dr. Kirk Gerdes and Dr. Shiwoo Lee for allowing me the time to develop and grow into the researcher I am today. Also, to all my colleagues who helped me during the process. Many thanks need to go to Mary Anne Alvin as well. All the idea's and decisions we've had helped to properly develop my project and the growth of my ability as a student researcher. Thanks also go to Mr. Rich Dennis for his support on this project. This project is sponsored by the Department of Energy under the RDS contract DE-FE-00040000.

I also send many thanks to my parents, Rich and Suzie Miller, and my brother, Matt. Without their love and support, I would not be in the position I am today.

My girlfriend Emily Abbondanza deserves much of the credit for my success in school. Her continual support and guidance has pushed me to great heights.

I'd like to dedicate this work to a loved one, Sam, I lost during this journey. I miss her very much, but I continue to work hard to make her proud.

1.0 INTRODUCTION

1.1 GAS TURBINES AND AIRFOIL COOLING

Though most people may not know what a turbine is or what it does, they rely on it regularly to support daily activities. Energy (land-based power) and aviation (aircraft propulsion) are two of the major applications that use gas turbines to create power. This is achieved by using hydrocarbon fuels to create thermal energy (from combustion), were the specific purpose of the gas turbine is to convert thermal energy into mechanical energy. This makes the goal of engineers working within thermal engine systems to achieve the highest efficiency possible, and now more than ever the push for increased performance is at the forefront of energy research.

As energy demands continue to rise and fuel supplies slowly dwindle, it is critical that gas turbine efficiency remain the top priority for turbine related research. To increase system efficiencies, operating temperatures must be increased while compressor consumption remains constant or decreases. Rotor Inlet Temperature, also referred to as Turbine Inlet Temperature, typically ranges from 1400°C to 1800°C [1]. Upstream of the turbine, combustion occurs at temperatures well over 2000°C, but must be cooled to protect the combustor liners and the turbine components. Increased compressor load and reduced in operating temperatures significantly affects the system efficiency. With current inlet temperatures at or exceeding the material limits, the widespread approach to increasing efficiency is with novel internal blade and

vane designs. How these cooling features affect the performance of the system can be seen in Figure 1[1].

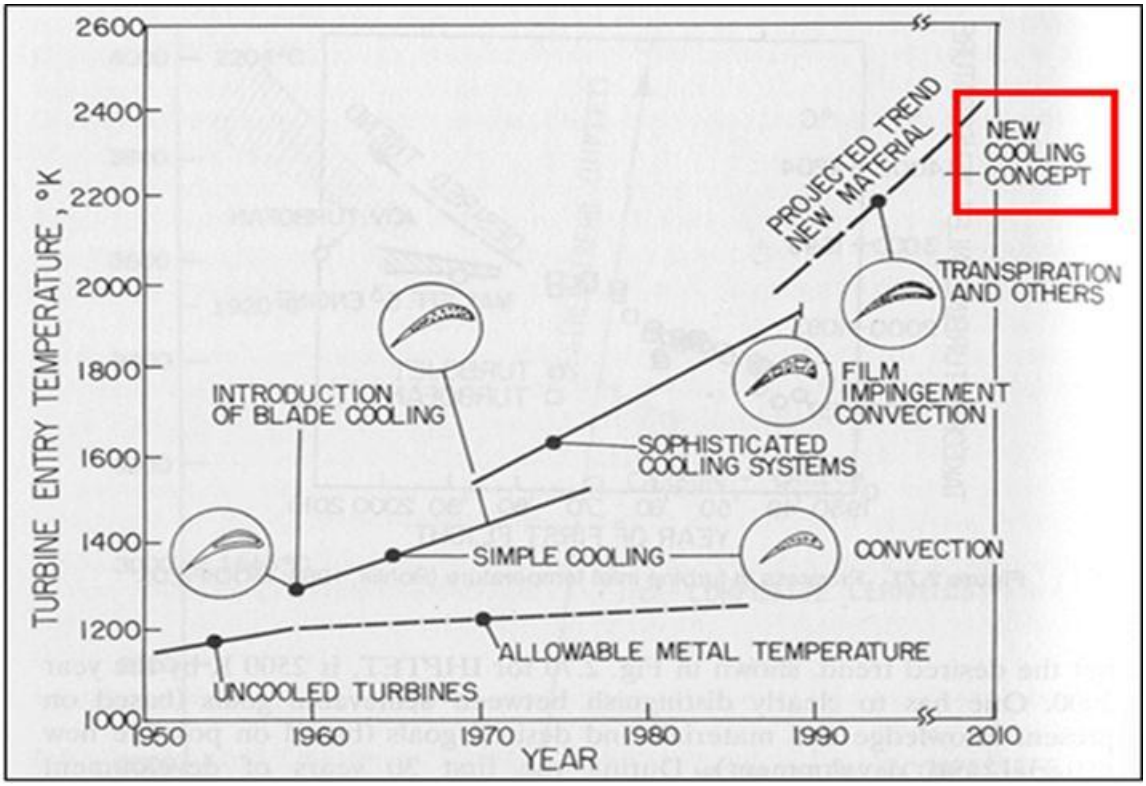

Figure 1. Gas Turbine Cooling Schemes as Presented Over the Past 60 Years [1]

As seen in Figure 1, when gas turbine systems were uncooled, operating temperatures peaked at 1200 K due to material melting points. The introduction of convection cooling and the development of sophisticated cooling schemes have greatly improved Turbine Inlet Temperatures. Gas turbine cooling technology can be divided into three categories: 1) thermal barrier coatings (TBC's), 2) external cooling and 3) internal cooling, which is the focus of this study. Thermal barrier coatings are used on the exterior of the turbine blade to act as insulation from the hot gas. As the TBC's are typically comprised of ceramic materials they provide good

insulation. Some additional coatings maybe used on the exterior, but are used more for protection against the metal oxidizing.

The majority of the protection provided to the airfoil is generated by the convection cooling of the internal and external features. Figure 2 [2] shows how the internal and external features are used together to maximize convection heat transfer.

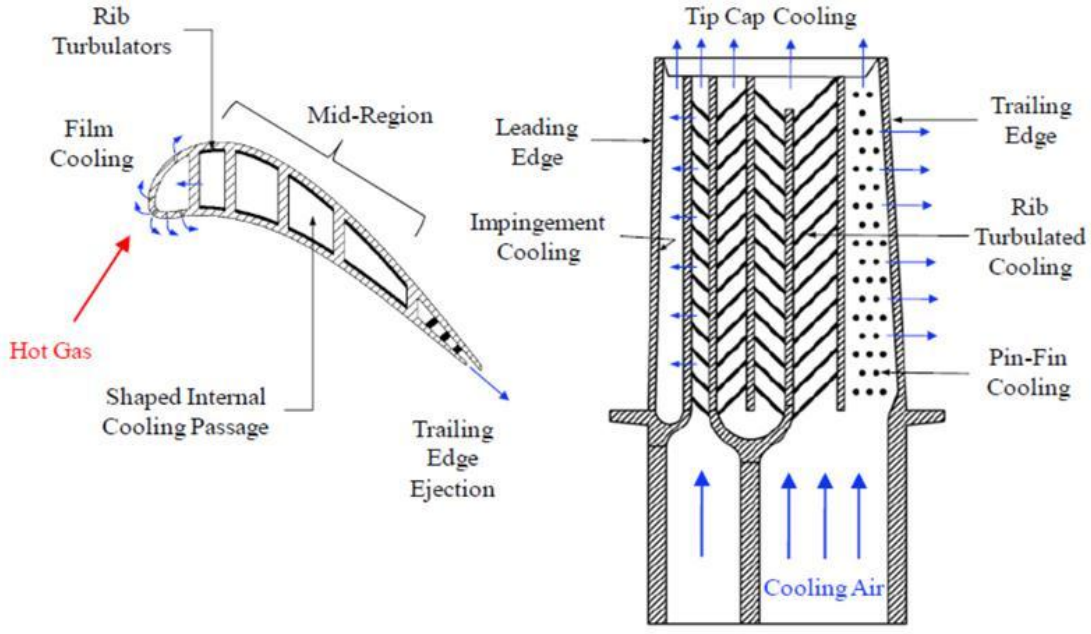

Figure 2. Conceptual View of Cooling Passages Size and Orientation [2]

In this particular case, the external cooling consists of the film cooling on the leading edge, while the internal cooling consists of jet impingement cooling in the leading edge, serpentine turbulated channels in the main body and pin fins in the trailing edge section. Jet impingement offers the best heat transfer and is typically employed in areas of high thermal load, i.e. the leading edge. With an array of many jets, jet to jet interaction can weaken jets and can be further deteriorated from crossflow effects. Using it with film cooling can be a benefit because

flow can be ejected, decreasing crossflow effects. The ejected air from the film cooling holes will remain close to the surface creating a protective boundary layer. In the main body and trailing edge sections, rib turbulators and pin fins are used to increase surface area and help promote better mixing. With more surface area and better mixing, high heat transfer is obtainable. Introducing turns into the channel continues to increase mixing. Pin fins not only help to relieve thermal stress, by offering better heat transfer, they also help to strength a very weak, small portion of the airfoil. Han et al. [3] have created a very informative collection of all the different varieties of turbine cooling.

Currently, gas turbine cooling is moving towards micro cooling by deploying a double wall cooling technique. Representing how the cooling schemes of past and present are different Figure 3 [4,5] shows the difference between two jet impingement airfoils. Bunker [6] has expressed the importance of moving to micro cooling, while Chyu and Alvin [7] and several patents show the importance of double wall cooling[8,9].

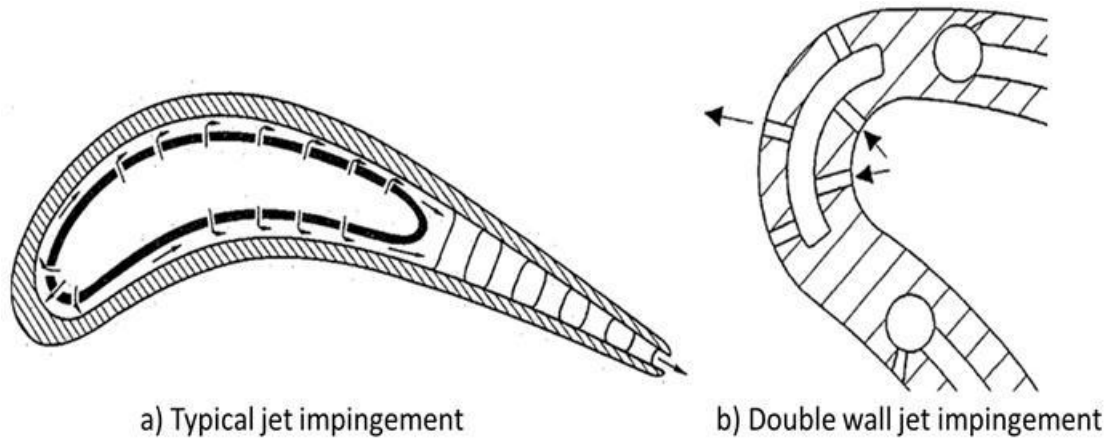

Figure 3. Difference Between Typical Cooling [4] and Double Wall Cooling [5]

Current technologies, specifically better casting techniques and additive manufacturing (3D printing) have made once improbable design idea's relevant. These advancements in manufacturing techniques allow for tighter tolerances and smaller features, providing room for cooling schemes to move closer to the external surface of a gas turbine blade. In these "near surface" cooling arrangements, jet impingement is able to thrive as it is most effective cooling technique applicable in areas of high thermal loads. Although jet impingement has an extensive history, spanning several decades and a variety of genres, it remains a complex topic do to its many influencing factors, such as jet geometry, channel geometry, crossflow, jet spacing, etc. Thus understanding the jet impingement requirements of each individual system is extremely imperative.

1.2 LITERATURE REVIEW OF JET IMPINGEMENT AIRFOIL COOLING

Jet impingement is used across several different regimes as a way to enhance heat transfer by offering greater surface area coverage, ultimately resulting in more uniform cooling. Its direct contact with the hot surface offers the optimal cooling scheme, whether cooling ceramics/glass, electronics, or gas turbine airfoils, which are the focus of this paper. These fields differ only in the way that the flow exits after impingement, either through four, two or one exit. In the case of the gas turbine airfoils, flow typically exhausts through 1 or 2 exits, meaning crossflow will be a contributing factor on the prevalence of the jets in the downstream regions. Intricate internal patterns coupled with jet impingement make for a very complex flow domain, thus the reasoning for why jet impingement research has spanned several decades.

Jet impingement is a very unique topic, in the sense that the intended setups are tailored to the individual's needs, giving it an extensive backlog of experimental and numerical results. Several review papers explaining the multiple paradigms of jet impingement exist [10-14]. Most papers related to airfoils study arrays of jets because it is necessary to understand the effects of crossflow, but some have taken studies to a more fundamental level and examined single jets. Martin [14] studied both circular and slotted single jets as well as multiple jet arrays. That particular study gave very detailed explanations of the flow characteristics of the single jet. A review by Livingood and Hrycak [15] also expressed significant results found in single jet studies.

As previously stated, jet impingement used in airfoil cooling typically has 1 or 2 exits, making crossflow a contributing factor to the flow characteristics. Obot and Trabold [16] discussed the three regimes of crossflow: minimum, intermediate and maximum. Although minimum crossflow would result in the best heat transfer enhancement, maximum crossflow channels are the most applicable to gas turbines, due to the way channels are arranged and how flow is fed to the jets. Hollworth and Cole [17] found that deflection of the downstream jets was how crossflow affected the jet impingement heat transfer. The crossflow becomes more effective as it propagates downstream, essentially resulting in heat transfer that is mainly dominated by convection instead of jet impingement.

Many techniques have been studied to attempt to combat the effects of the crossflow, like jet-to-wall separation distance *H/D*, jet-to-jet spacing S/D in both the streamwise and spanwise directions and impingement inclination/direction. The separation distance is the ratio of the distance between the jet plate and target plate, *H*, and the jet diameter, *D*. It has been generally accepted that for an array of multiple jets that this value be between 1 and 3 [10,13]. Goldstein

and Seol [18] concluded that this was a result of a short jet core length. Jet-to-jet spacing is another key component to optimizing jet impingement heat transfer as most practical designs form some version of an array. Jets spaced too far apart will act like a single jet, as found by Goodro et al. [19] and provide a non-uniform cooling coverage. Jets spaced too close to each other, or to a wall, will create areas of entrainment, decreasing the effectiveness of the jet. It has become come practice to have an S/D value of no greater than 10 diameters, but 4-6 diameters will offer heat transfer optimization [17].

Others have studied varying jet diameters as a way to negate crossflow effects. Uysal et al. [20] explored the effects of varying jet diameters in an inline jet array using the transient liquid crystal technique. It was found that by increasing the downstream jet diameters, while decreasing the upstream jet diameters, one could minimize the effects of the crossflow.

Angled impingement has also been studied, as shown by Huang et al. [21] and El-Gabry and Kaminski [22]. Both studies show that with jets angled (30º,45º or 60º) in the streamwise directions, upstream or downstream, heat transfer is much less than that of the orthogonal jets. When jets are angled upstream, the crossflow will diffuse the impingement effect [3] and when jets are angled downstream, the crossflow will tend to deflect jets greater and wash flow away. The present study differs by implementing jets that are angled in the spanwise direction.

The presence of surface roughness on the target plate has also been studied [23-29]. The presence of ribs can enhance the heat transfer of the jet array, but it has been reported that higher heat transfer enhancement is observed in the downstream, while the upstream jet heat transfer enhancement could diminish in the presence of ribs [24]. Thus, the location of the ribs is extremely important, as found by Chang et al. [27-29].

Additional novel ideas have been presented on jet impingement channels with “zero crossflow” by Ekkad et al [30] and Lee et al. [31]. The idea presented by Ekkad et al., seen in Figure 4, suggests increasing the jet height, with upstream jets being the shortest and increase height moving towards the downstream. Even with increasing crossflow effects as the flow propagates downstream the impingement effect is largely preserved.

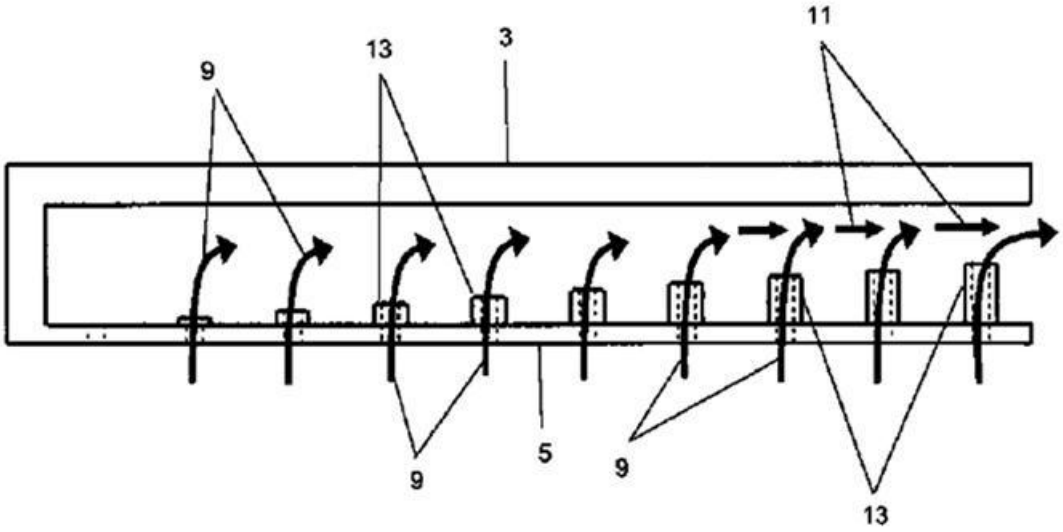

Figure 4. “Zero Crossflow” Jet Impingement US Patent 8,127,553 B2 [30]

To fully understand the flow characteristics in the present study due to jet impingement, numerical analysis are performed. This can be extremely difficult for impingement because of the jet-to-jet interaction and because of the effects of crossflow. These effects within the model tend to lead to over predicted heat transfer on the target surfaces. The turbulence model that is typically employed is the k-ε model with scalable wall functions. One of the major concerns with k-ε turbulence model is that it tends to over-predict heat transfer enhancement [10]. This has lead others to start using the v2f model [32] or the SST model [33,34]. For this study, the SST model is used to explore the flow characteristics in the channel.

1.3 PRESENT STUDY STATEMENT

The work presented in this study is to represent a scaled up model of a micro jet channel that is applicable to the internal cooling design of gas turbine airfoils. The goal of these experiments was to optimize the heat transfer enhancement of the jet channel. This was accomplished by examining three individual topics: 1) varying flow/varying diameter jet plates, 2) staggering and inclination of jets and 3) deploying surface roughness on the jet channel target plate. These experiments were all conducted using the well-established transient liquid crystal technique. Starting with the varying flow test, it could be properly analyzed how each jet flow affected the heat transfer of the channel. Initially conducting tests where all jet flows were identical, flows could then be varied to optimize the heat transfer of the channel.

Though the varying flow can show the optimal flow range of each jet, it is not realistic of an actual jet impingement array. In a typical array, all jets are fed by one centralized plenum and to adequately test the effects of the optimal varying flow case, a varying diameter jet plate that is plenum fed was designed.

To further investigate the optimization of the jet channel, jet staggering and inclination was examined. By staggering jets, jet to jet interactions and the effects of crossflow can differ from that of the inline jet array. Jet plates were designed to be staggered 1D and 2D. Also, to understand how impingement angle affects the effectiveness of the jet, jet plates were designed with jets angled at 30º, in the spanwise direction, while maintaining the 1D and 2D staggering. To the author's knowledge, no other studies have researched angled jets impinging in the manner.

The final set of scaled up tests involved introducing surface roughness on the channel target plate. As explained in the previous sections, rib turbulators increase the surface area

available for heat transfer while helping to promote better mixing. These effects were studied using the baseline inline jet array.

Numerical analysis using ANSYS CFX 14.0 was explored to understand the heat transfer and fluid flow within the jet channel. By comparing numerical heat transfer to the experimental cases, our studies can be validated while learning how fluid flow within the channel affects the heat transfer. Understanding the flow in the fluid domain was the major focus of the numerical studies.

The last study presented is a scaled down representation of the jet channel studied in the aforementioned studies. In the previous studies, just one jet channel was explored at a scaled up level, but using the scaled down model allows the effects to be seen at a more realistic level by implementing several jet channels. Using a stainless steel coupon, the target surface was held at a constant temperature and by monitoring inlet and exit temperatures the average heat transfer was found. These results were then compared to results found in the literature.

2.0 EXPERIMENTAL SETUP AND ANALYSIS

2.1 TESTING PROCEDURE

Compressed air is directed through a pressure regulator where pressure is be maintained at approximately 80 psi. Prior to the experiment, air is heated to the desired temperature (approximately 60^{o}C), by using a series of inline heaters connected to a variable transformer. During the heating period, hot air is directed to 5 individual flow meters, which measure the volumetric flow rate. The flow rate to each meter is controlled by a brass globe valve, which is directly upstream of the flow meter. Downstream of the flow meters hot air is directed to bypass valves, where temperature is measured using a digital thermometer connected to Type K Thermocouples. When the air temperature reaches a steady state condition (approximately 55^{o}C), hot air is then directed into the test section. Figure 5 presents the entire test setup used for this experimental study. Simultaneously, images of the test domain showing the temperature history versus time are captured by using a charged-couple-device (CCD) camera mounted perpendicular to the test domain. Type-K thermocouples are used to monitor and record the temperature history of the entire test domain via the data acquisition system. At the inlet and outlet of the jet channel, two thermocouples are inserted up to the mid-plane of the flow domain to measure the temperature of the bulk flow. The bulk temperature of the entire test domain is determined by linear interpolation between the temperature profiles recorded at the upstream and

downstream during the entire experiment. All thermocouples are connected to a National Instruments SCXI 1000 Chassis via an NI SCXI 1303 terminal block. To characterize the pressure loss in the jet channel, measurements are recorded immediately after the heat transfer tests, using pressure taps installed at the same locations of the thermocouples and connecting to a hand held digital manometer.

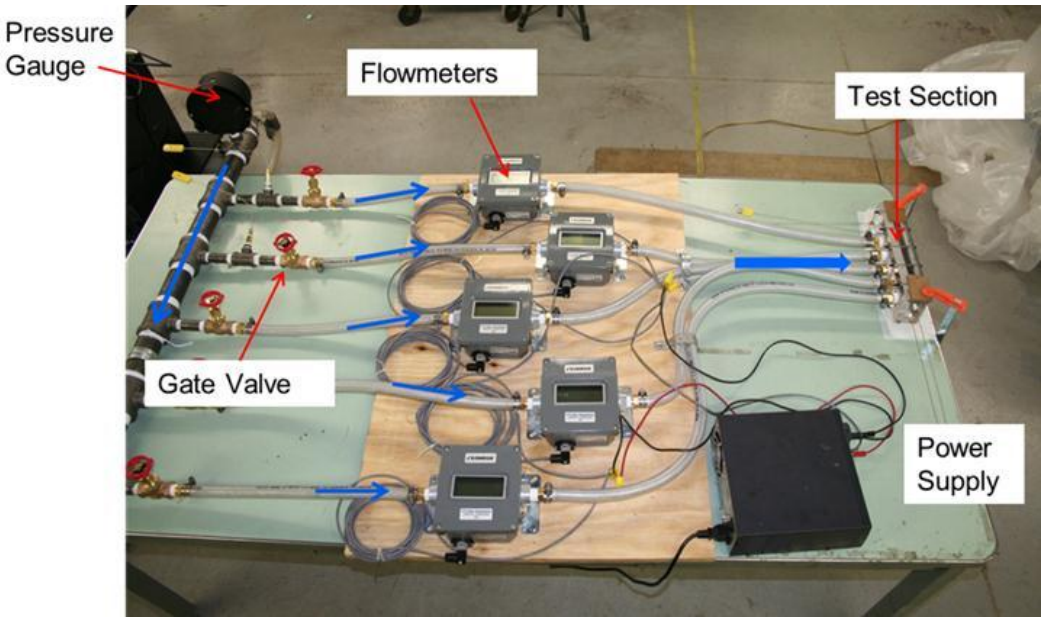

Figure 5. Schematic Layout of Testing Setup for Liquid Crystal Technique

2.2 JET IMPINGEMENT TEST CHANNELS

All test sections were machined from Plexiglas, which exhibits low thermal conductivity and is crucial to ensure the validity of the one-dimensional, semi-infinite heat transfer model on which the local heat transfer coefficient for the target surfaces are determined.

The baseline cases for all experiments had jets of constant diameter, 9.53 mm (0.375 in). The baseline case has a height-to-diameter ratio, *H/D*, of 2 and jet-to-jet spacing to diameter ratio, *S/D*, of 4. Channel height and width are held constant for all cases.

2.2.1 Varying Flow Channel

The test section is a rectangular channel that is 254 mm x 57.15 mm (10.0 in x 2.25 in), consisting of a jet plate of 19.05 mm (0.75 in) thick and target plate 12.7 mm (0.5 in) thick. The jet plate contained 5 jets, all tapped to fit a 12.7 mm (0.5 in) NPT fitting, which has an ID of 9.53 mm (0.375 in). The entire jet channel assembly is illustrated in Figure 6. Table 1 summarizes the flow rates used for each jet during these test cases.

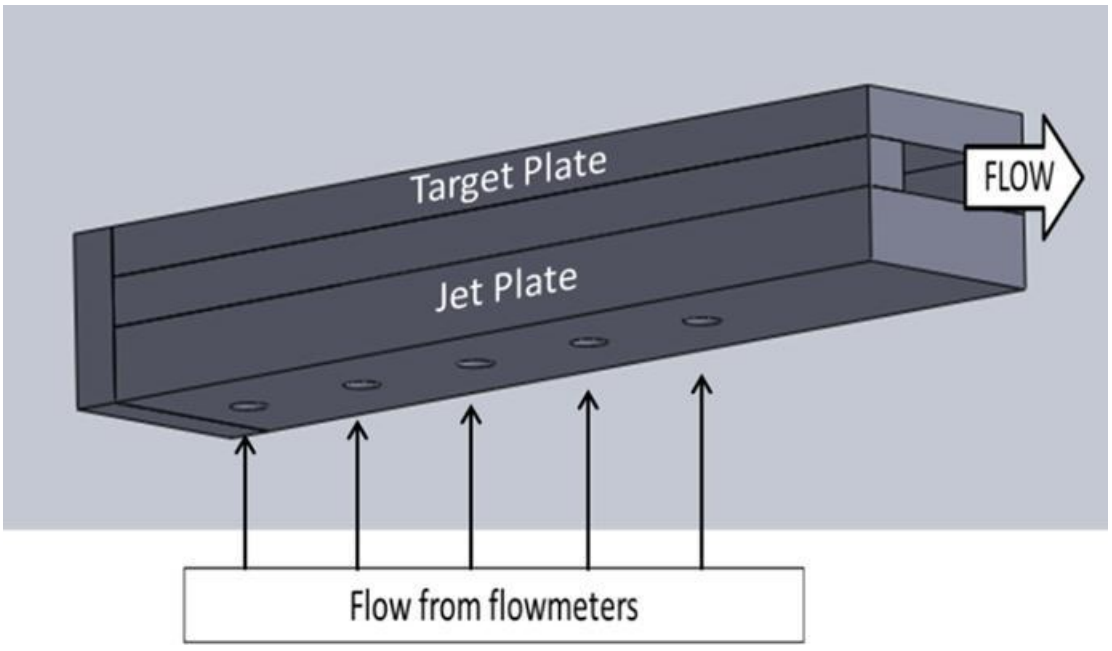

Figure 6. Three Dimensional Representation of Varying Flow Channel

Table 1. Jet Reynolds Number for Varying Flow Test Cases

	Jet 1	Jet 2	Jet 3	Jet 4	Jet 5
Baseline	67,000	67,000	67,000	67,000	67,000
Test 1	74,000	67,000	67,000	67,000	74,000
Test 2	74,000	67,000	60,000	67,000	74,000
Test 3	74,000	67,000	47,000	67,000	74,000
Test 4	74,000	67,000	0	67,000	74,000
Test 5	74,000	74,000	67,000	67,000	74,000
Test 6	67,000	53,000	67,000	53,000	67,000

2.2.2 Plenum Fed Jet Channel

The plenum in these experiments was 190.5 mm (7.5 in) x 57.1 mm (2.25 in) x 50.4 mm (2.0 in). The entire test section is illustrated in Figure 7. The jet impingement channel is a rectangular channel that is 254 mm x 57.15 mm (10.0 in x 2.25 in), using a jet plate of 19.05 mm (0.75 in) thick and target plate 12.7 mm (0.5 in) thick.

Table 2 summarizes the varying diameter jet plates that were explored in this study. For reference, Test SB's diameters were found after completing the baseline study of these current tests. SB stands for small to big, as in small upstream diameters to big downstream diameters.

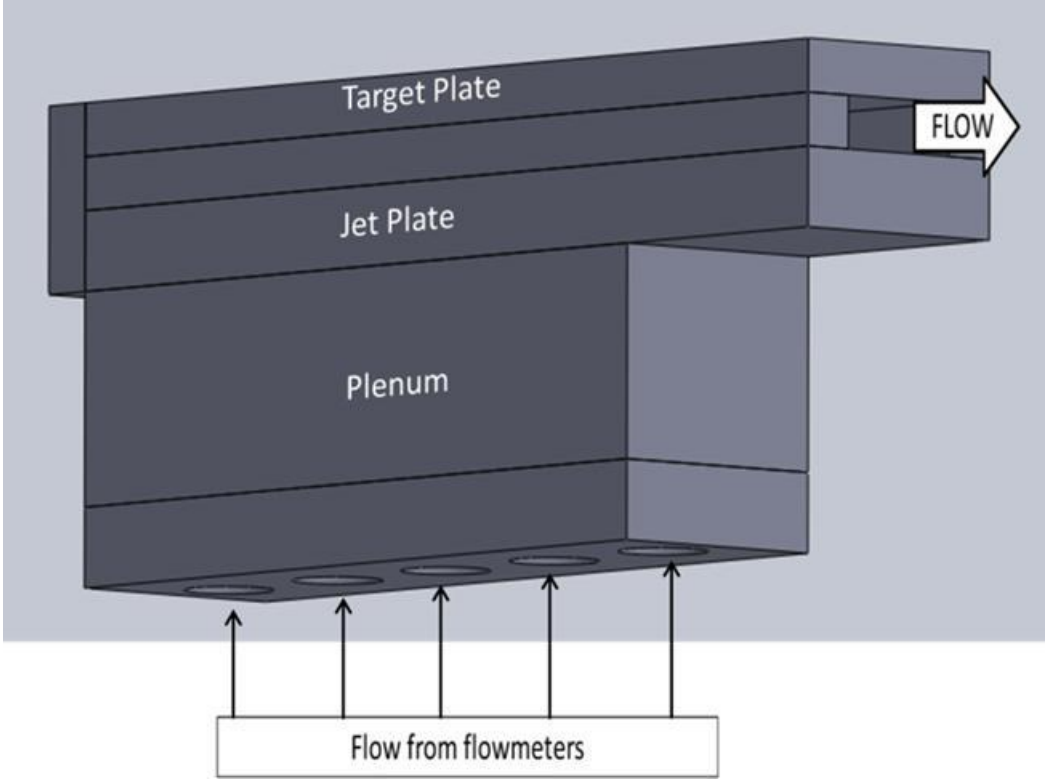

Figure 7. Three Dimensional Representation of Plenum Fed Jet Channel

Table 2. Diameter Sizes for Varying Diameter Test Cases

	Jet 1 Dia. (mm)	Jet 2 Dia. (mm)	Jet 3 Dia. (mm)	Jet 4 Dia. (mm)	Jet 5 Dia. (mm)
Baseline	9.5	9.5	9.5	9.5	9.5
Test 5	8.7	8.7	9.5	9.5	8.7
Test SB	8.7	8.7	9.5	11.1	12.7

Staggered jet cases consisted of jet plates with 1 diameter and 2 diameter spacing, jet center to jet center, in the spanwise direction. Jets for the staggered cases remained at 90°. Inclined (angled) jet cases also consisted of jet plates with 1 diameter and 2 diameter spacing in the spanwise direction. Jets for the inclined cases were angled at 30°. For the angled cases, jets

1, 3 and 5 are all angled towards the right side wall, while jets 2 and 4 were angled towards the left side wall. The jet plate that was considered the baseline case had all jets inline and 90°.

All rib cases tested in these experiments used the baseline jet plate. Figure 8 shows the different target plates, 90 degree ribs, chevrons and X's, which were made by an SLA process. All had a height and width of 3.175 mm (0.125 in). The rib-pitch-to-height ratio, *p/e* for the 90 degree ribs and chevrons is 11, while the X case is 12. The angles between legs of the chevrons and X's was 45 degrees. For the rib and chevron rib cases, features were placed 19.05 mm (0.75 in) downstream of each jet. For the X-shaped rib case, features were placed directly over top of the jets. The length of the 90 degree ribs was 55 mm (2.15 in), roughly the width of the channel. The chevrons had a length of 30 mm (1.2 in), while the X's had a length of 47 mm (1.85 in).

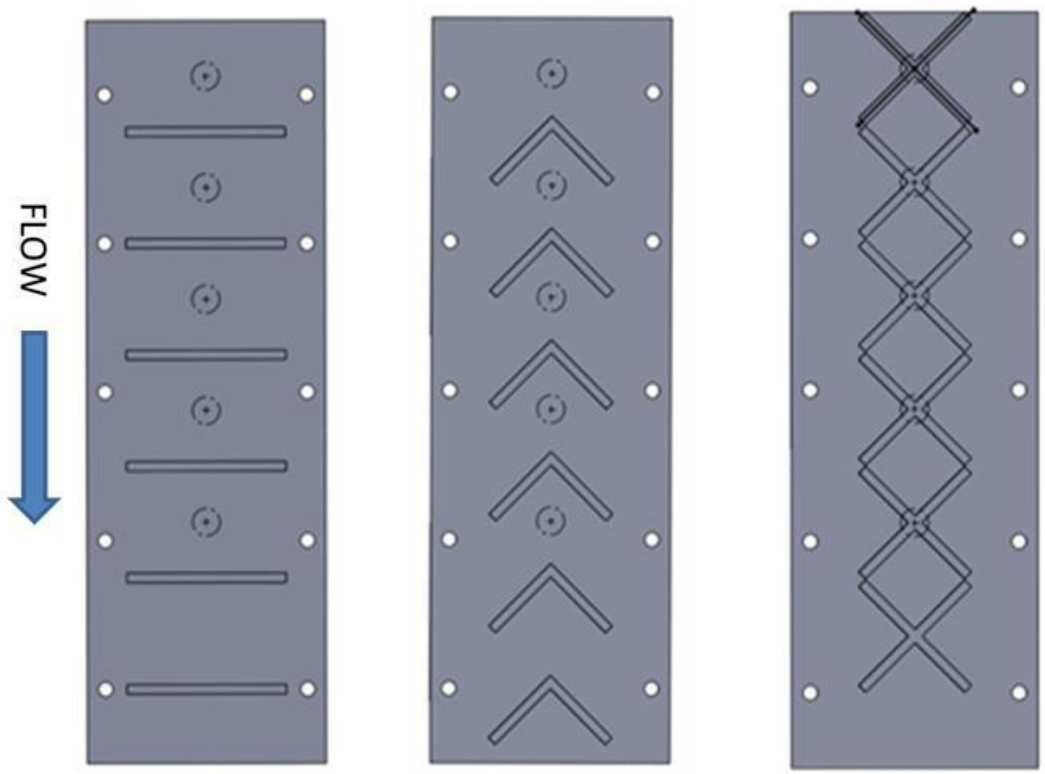

Figure 8. Target Plate Rib Designs used for Plenum Fed Jet Tests

2.3 DATA ANALYSIS

The Reynolds number, based on the jet channel hydraulic diameter (D_h), and the bulk mean velocity (U), which is calculated by using the total mass flow rate and the total area of the channel, is expressed below from 50,000 to 80,000.

$$Re = \frac{\rho U D_h}{\mu} \quad (2.1)$$

To resolve the heat transfer characteristics for the target plate and cases with rib turbulators, the current measurement approach is based on an established technique that is well documented by Chen et al. and Chyu et al. [35,36]. The results presented in this paper are in the form of a dimensionless heat transfer coefficient, the Nusselt number, Nu, which is defined as:

$$Nu = \frac{hD_h}{k} \quad (2.2)$$

Properties of air are taken based on bulk mean air temperature. The estimated uncertainty temperature measurement is 0.5^oC. The uncertainty analysis with a 95% confidence level on the Nusselt number ratio based on the method of Kline and McClintock [14] is approximately 8%. The uncertainty for pressure measurement is approximately 7%.

Total heat transfer enhancement for the jet arrays normalized by the fully developed smooth channel based on the Dittus-Boelter correlation:

$$Nu_0 = 0.023 Re^{0.8} Pr^{0.4} \quad (2.3)$$

Heat transfer enhancement is always penalized by the pressure loss in the system. The pressure loss characteristics of all jet plates are based on f/f_0, where f is the friction factor, defined by:

$$f = \frac{\left(dP/dx\right)D_h}{\rho\left(U^2/2\right)} \qquad (2.4)$$

and f_0 is the overall friction factor normalized by the corresponding data for fully developed flow in a smooth channel developed by Petukhov:

$$f_0 = (0.790 \ln Re - 1.64)^{-2} \qquad (2.5)$$
$$3000 \leq Re \leq 5x10^6$$

Dp/dx represents the pressure drop across the jet channel by measuring the static pressure of the plenum compared to atmospheric pressure.

2.4 STAINLESS STEEL COUPON

Compressed air is directed through a pressure regulator where pressure is be maintained at approximately 80 psi. Prior to the experiment, room temperature air is directed to a flow meter, which measures the volumetric flow rate. The flow rate to the meter is controlled by a brass globe valve, which is directly upstream of the flow meter. Once flow entered the test piece, several PVC rings were connected together to transition flow to the opening of the coupon. A heater is positioned on the target surface and current (I) is supplied by a power source. When all temperatures, inlet, exit and surface, reach a steady state condition, testing temperatures can be recorded. Figure 9 presents the entire test setup used for this experimental study. Figure 10 shows the PVC test chamber that houses the coupon and the heater.

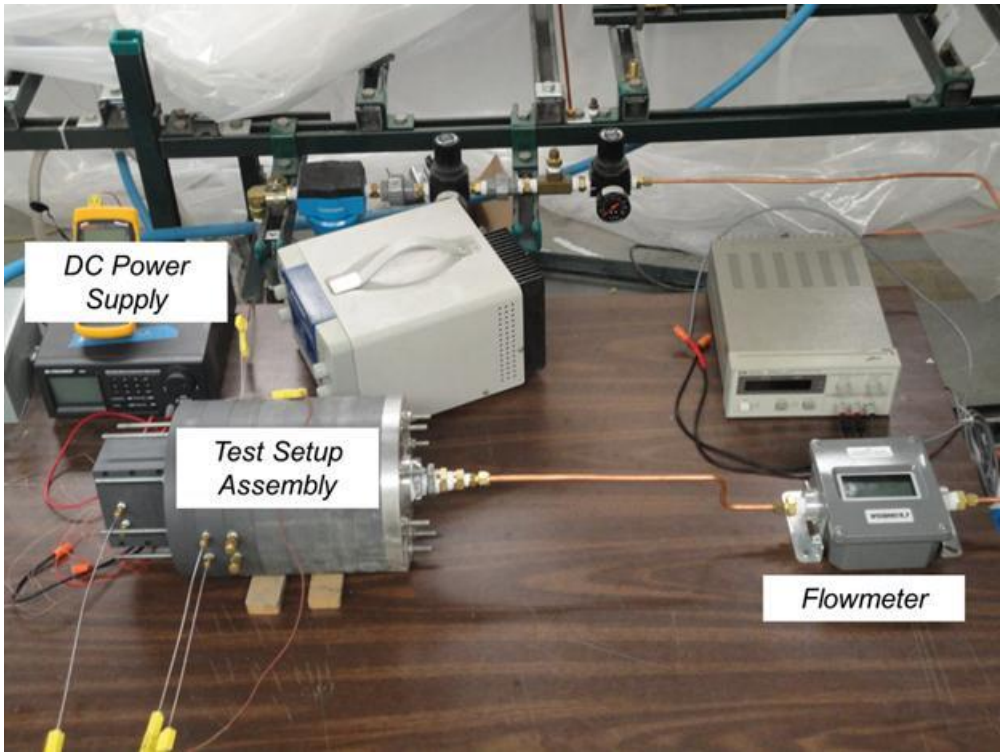

Figure 9. Schematic Layout of Testing Setup for Steady State Coupon Testing

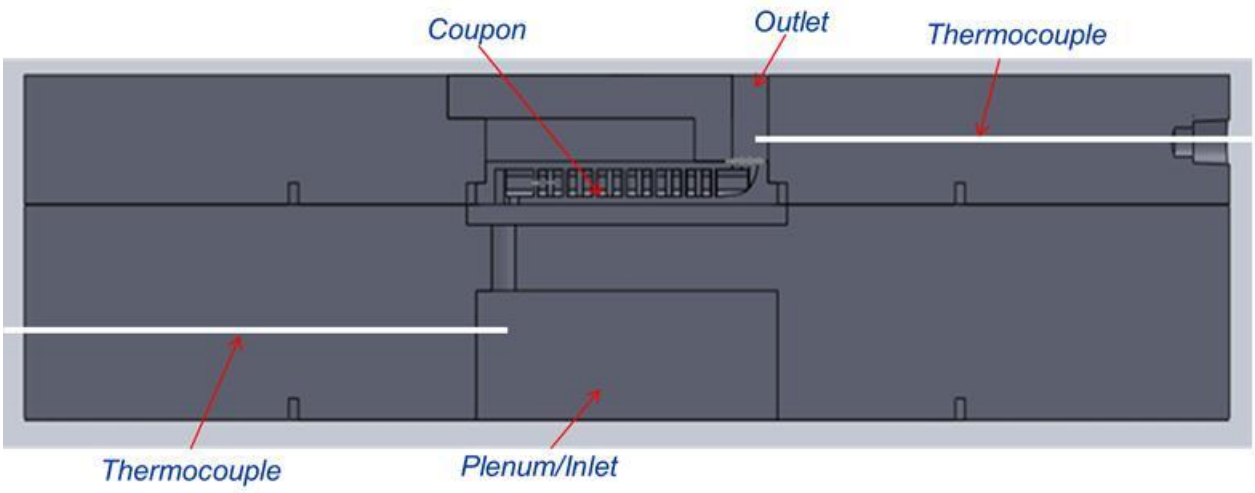

Figure 10. PVC Chamber that Houses Coupon and Heater

Type-K thermocouples are used to monitor and record the temperature history of the entire test domain via the data acquisition system. At the inlet and outlet of the coupon, two thermocouples are inserted up to the mid-plane of the flow domain to measure the temperature of the bulk flow. Four surface thermocouples are positioned between the heat and coupon surface. All thermocouples are connected to a National Instruments SCXI 1000 Chassis via an NI SCXI 1303 terminal block. To ensure temperatures had reached steady state, at least one hour was given for temperatures to stabilize. Over the time of that hour, several temperature data files were recorded and compared to ensure steady state. To characterize the pressure loss in the coupon, measurements are recorded immediately after the heat transfer tests, using pressure taps installed at the same locations of the thermocouples and connecting to a hand held digital manometer.

The coupon, machined from stainless steel (SS316), has external dimensions of 50.8 mm (2 in) x 50.8 mm (2 in). The coupon has 7 jet channels with 9 jets in each channel. Jet to jet

spacing, S/D = 4, with a diameter, D, of 1 mm. Jet to wall spacing is 1.5 mm, with a wall thickness of 3 mm. Two different coupons were designed, one with an H/D = 1 and the other with an H/D = 2. To be able to machine the jet channels, a lid had to be machined separately. A recess was machined into the coupon to be able to house the 1 mm thick lid. To secure each lid in place and make a leak proof seal, JB Weld epoxy for steel was used. Each coupon also had its own plenum machine into the bottom. The coupon can be seen in Figure 11.

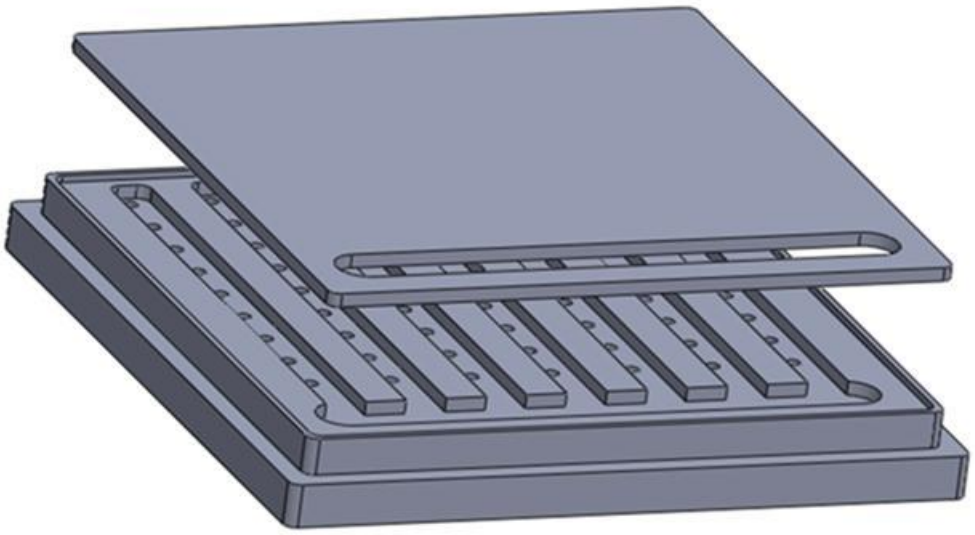

Figure 11. Three Dimensional Schematic of Jet Coupon and Lid

The heat transfer available in each jet coupon can be calculated by knowing the heat flux, area and the temperature difference:

$$h = \frac{q"}{A_{footprint} * \Delta T_{LM}} \qquad (2.6)$$

For these experiments, q" was found by multiplying the voltage (V) and the current (I). The footprint area is the area of the lid and the log mean temperature is found by:

$$\Delta T_{LM} = \frac{\Delta T_A - \Delta T_B}{ln\left(\frac{\Delta T_A}{\Delta T_B}\right)} \qquad (2.7)$$

The Reynolds number, which was previously expressed in equation 2.1 is based on the jet hydraulic diameter (D_h) and the mean jet velocity (U), which is calculated by using the jet mass flow rate and the area of the jet, ranges from 4,000 to 10,000.

Total heat transfer enhancement for the jet coupons normalized by the fully developed smooth channel is based on the Dittus-Boelter correlation, previously expressed in equation 2.3.

The pressure loss characteristics of both jet coupons are based on f/f_0, where f is the friction factor and f_0 is the overall friction factor normalized by the corresponding data for fully developed flow in a smooth channel developed by Petukhov. Both equations were previously described, eq. 2.4 and 2.5.

3.0 NUMERICAL MODEL

3.1 SETUP AND BOUNDARY CONDITIONS

Numerical analysis was conducted using ANSYS CFX version 14.0. The flow domain is the same as described in the experimental section, for varying flows and plenum fed jet plates (surface roughness was not explored numerically). CFX Meshing was used to create the meshes, consisting of approximately 800,000 elements for the varying flow case and 2,000,000 for the plenum fed jet plates, and to impose an inflation layer on the target plate. The boundary conditions for all numerical cases are set to be the same with inlet air temperature maintained at 350 K and the target plate and surround jet channel walls are constant at 300 K. The remaining wetted areas, jet walls and plenum walls in the varying diameter case, are also set at 300 K. The inlet velocities were obtained from the flow rates used during the experimental tests. The pressure at the exit is set to atmospheric. For these numerical investigations SST (Shear Stress Transport) was used as the turbulence model.

In all calculations, the root-mean-square (rms) and maximum absolute errors for both the mean flow and turbulence quantities were monitored for each computational block to ensure complete convergence of the numerical solutions and a convergence of 10^{-5} was used for the maximum rms error.

4.0 HEAT TRANSFER EFFECTS OF VARYING FLOW JET IMPINGEMENT

4.1 LOCAL HEAT TRANSFER COEFFICIENT

The heat transfer coefficient distribution in the channel is mainly governed by two competing phenomena, 1) impingement and 2) the development of cross-flow towards the downstream region. Heat transfer at the upstream region is mainly dominated by the impingement effects, while the cross-flow effects become more pronounced as the flow propagates downstream. Figure 12 shows a comparison of the local heat transfer coefficient, h, distribution of the baseline case (uniform flow rate) and some of the test cases with varying jet flow rates in this study, presented in Table 1. Examining each jet individually, the highest heat transfer occurs where the jet impinges; essentially, where the core of the jet has the highest velocity and impinges with the greatest impact. As the flow moves out radially, heat transfer decreases as an effect of the outer edges of the jet having less impact on the target plate. Heat transfer in the radial direction is also affected by jet-to-jet interaction, as will be discussed in more detail based on the numerical findings. This is very evident in the baseline case, as illustrated in Figure 12. Jet 1, jet most to the left, is next to the end wall and has Jet 2 on its right. Because of the entrainment caused by its close proximity to the end wall and to the interaction/entrainment caused by Jet 2, Jet 1 has a lower heat transfer. The same can be said for the performance of Jet 2, as it interacts with Jet 1 and Jet 3, the center jet in the array. A different story arises for the performance of Jet 3.

Although it too is between two jets, Jet 2 and 4, it shows the highest performance. This happens because the interaction with Jet 4 is weak, due to it being deflected downstream by the crossflow. Jet 4 has similar interactions with Jets 3 and 5 due to the stronger presence of the crossflow in the downstream regions. As the crossflow effect increases towards the downstream, Jet 5 experienced the lowest heat transfer performance as the impingement effect decreases significantly. In addition, stronger crossflow effect may have also deflected the jet stream.

Figure 12 also illustrates the local heat transfer coefficient distribution of all varying flow test cases in the present study. In Test 1, 2, 3 and 4, the flow rates for both Jet 1 and 5 are higher than the baseline case by approximately 10%, while varying the flow to Jet 3 in a rather significant range, to the point where it is completely shut off. The results shown in Figure 12 suggested that increasing the flow rate to a particular jet resulted in stronger impingement effects, having a pronounced impact towards the heat transfer performance on the target plate. With higher velocity, the coolant in the upstream regions of the channel impinged with greater force and in the downstream regions managed to overcome deflection caused by the crossflow, providing stronger impingement and ultimately resulting in higher heat transfer performance.

This is revealed in Test1, 2 and 3, whereby the heat transfer subjected to impingement from Jet 1 and Jet 5 is higher than the baseline case. Reducing the flow to Jet 3, changing the jet Re from 67,000 to 60,000 does not appear to have much contribution to the heat transfer performance as both Test 1 and 2 appear to be quite comparable. However, when the jet Re for Jet 3 is further reduced to 47,000 (approximately 30% reduction compared to the baseline), this has enhanced the impingement effect of neighboring jets (Jet 2 and 4), while simultaneously reducing the inter-jet interaction. For Test 4, shutting off Jet 3 does not appear to be a good option as the heat transfer is substantially low without the impingement, creating a hot spot that

will eventually lead to higher thermal stress. Overall, Test 5 has the best heat transfer performance among all tested cases, were the relatively weaker jets (1, 2 and 5) all have increased flows compared to jet 3 and 4.

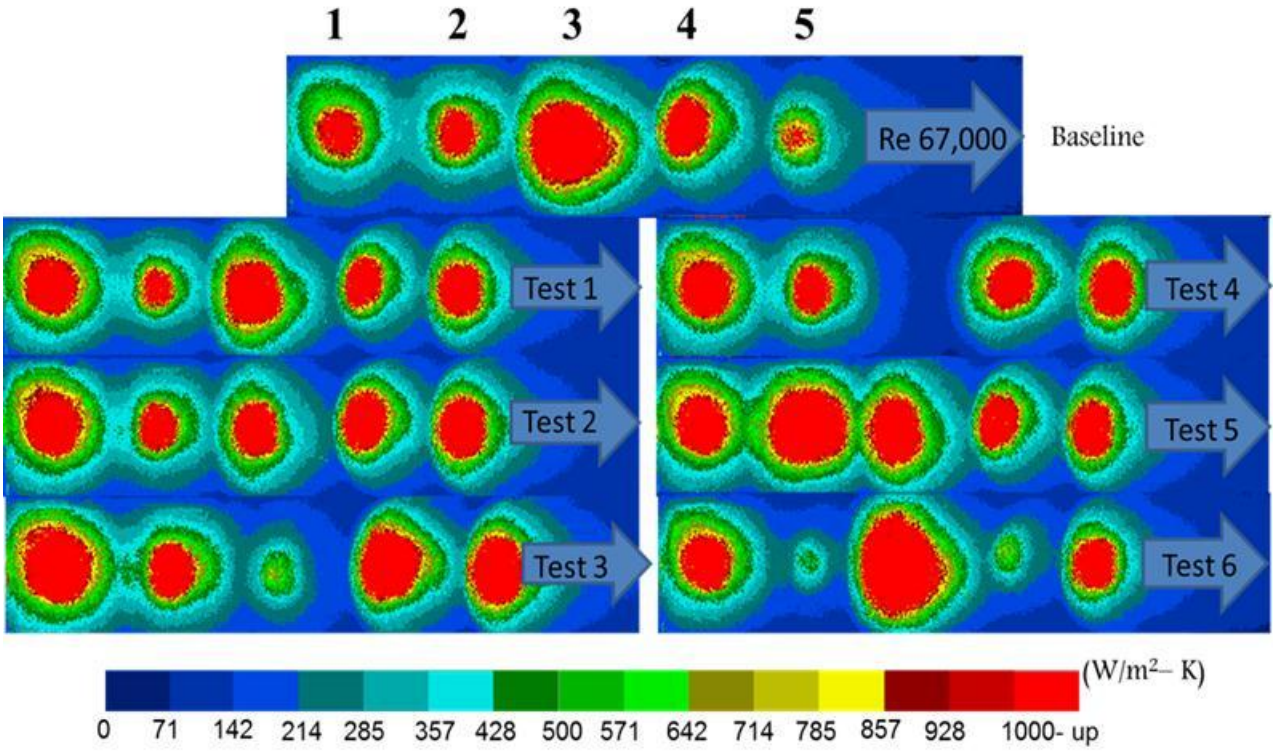

Figure 12. Local Heat Transfer Coefficient for Baseline and Varying Flow Cases

4.2 SPANWISE AVERGAED HEAT TRANSFER

Figure 13 and 14 illustrate the averaged spanwise distribution of all test cases. In Figure 13, with less crossflow effects, the peak heat transfer of varying magnitude under Jet 1 and 2 is largely preserved for all test cases. Compared to the baseline case, by increasing the jet Re for Jet 1 and 2 by approximately 10%, heat transfer is further enhanced ranging from 20-80%. Understandably

that with low flow and without jet impingement in Jet 3 in both test 3 and 4, heat transfer decreases significantly in those region. For the baseline case, lowest peak heat transfer is observed at the downstream due to the increasing crossflow effect. However, test 3, 4 and 5 revealed an opposite trend when flow rate is increase by approximately 10%. An interesting phenomenon is observed in test 3, where Jet 4 and 5 are deflected further downstream compared to other cases. One plausible reason that could contributed to such a phenomena is that Jet 3, which has lower bulk flow velocity, cannot impinge onto the target plate, therefore, the main fraction of the flow coming out of Jet 3 is being pushed downstream deflecting Jet 4 and 5.

In Figure 14 both test 1 and 2 exhibit higher heat transfer performance than the baseline case when flow for any particular jet is increased. The result of Test 6 as shown in Fig. 14 confirmed the findings in Fig.12 that by alternating the magnitude of jet in such a pattern does not appear to be a viable option, which only resulted in periodic peak heat transfer in the flow domain.

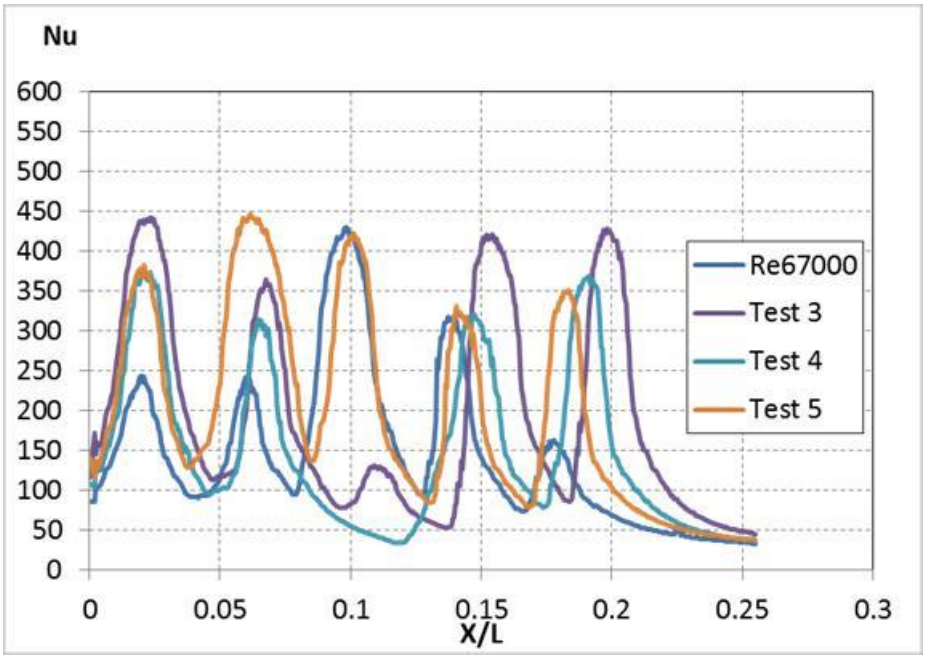

Figure 13. Spanwise Averaged Heat Transfer for Baseline and Varying Flow Cases 3, 4 and 5

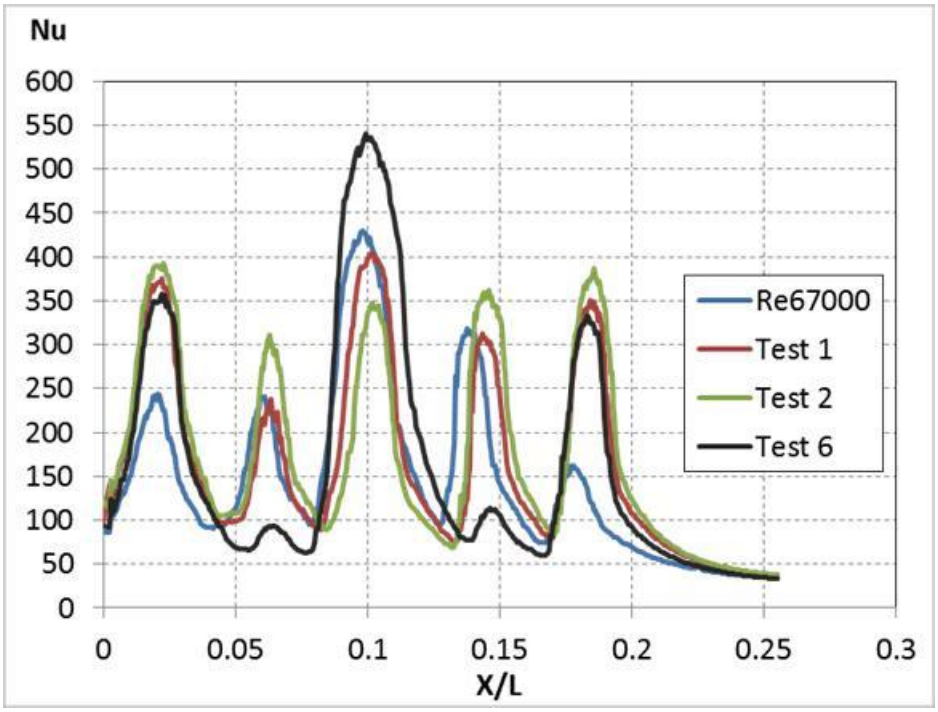

Figure 14. Spanwise Averaged Heat Transfer for Baseline and Varying Flow Cases 1, 2 and 6

4.3 TOTAL HEAT TRANSFER ENHANCEMENT

These results are further solidified in Figure 15, which illustrates the total heat transfer enhancement for the baseline and varying flow rates normalized by the fully developed smooth channel based on the Dittus-Boelter correlation. By normalizing the Re of the channel in each test, one could compare the enhancement of the varying cases to the baseline. It is seen that with a change of ±2% to the channel Re, that the flow rates used in Test 3 and Test 5 could increase the performance by 35%. In some cases, the total enhancement can be less than one because of the way heat transfer was averaged for Nu_T. The whole target plate domain was used to find an average heat transfer. The low heat transfer areas outside of the impingement location make the enhancement seem less than it really is.

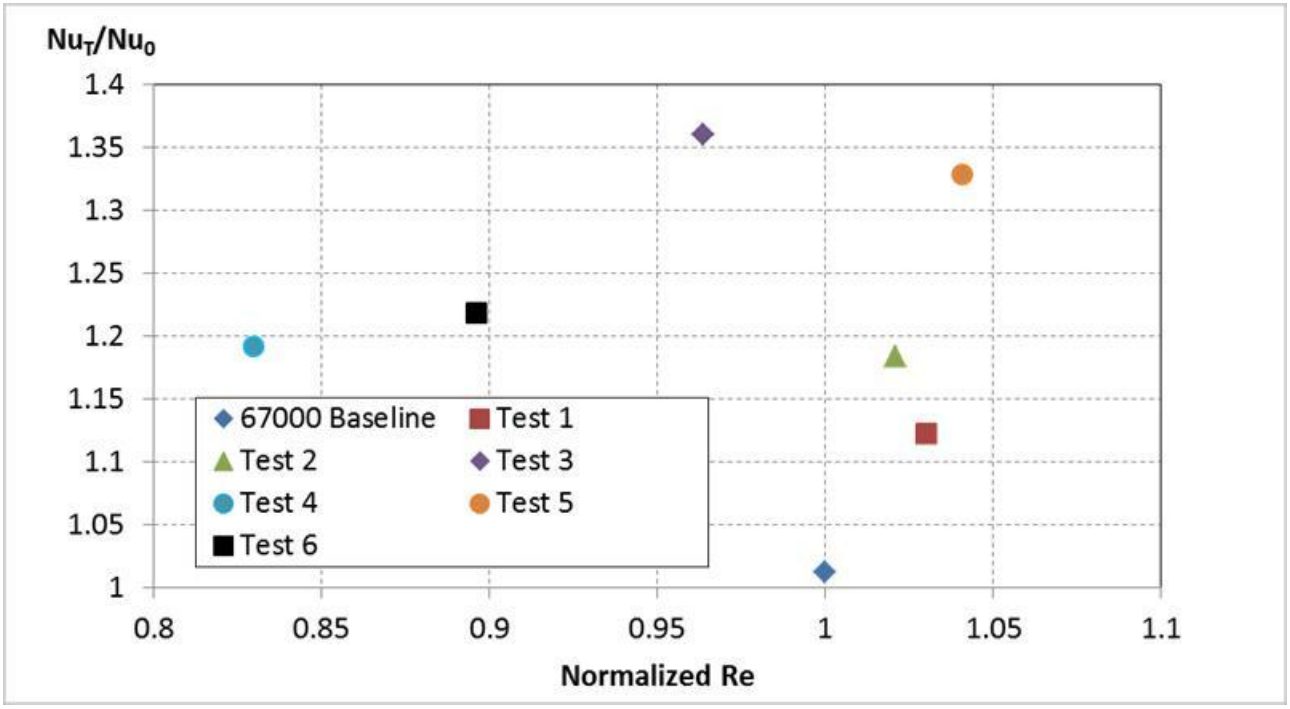

Figure 15. Total Heat Transfer Enhancement for Baseline and all Varying Flow Cases

4.4 NUMERICAL RESULTS

The mesh for the varying flow cases consists of approximately 800,000 elements with the first cell normal to the wall corresponding to a y+ value ≤ 2. Figure 16 shows a comparison of the experimental and numerical local heat transfer coefficients. Qualitatively, both numerical and experimental results are in good agreement. Based on Figure 16, both results revealed that the heat transfer performance caused by jets 3, 4 and 5 is affected by the crossflow. Jet 2 also shows signs of being affected by jets 1 and 3. The heat transfer coefficient found numerically is under predicted compared to the experimental case, except for jets 4 and 5. For jets 1 and 2, higher heat transfer occurs in stagnation zones, but for jets 3, 4 and 5 it occurs in the upstream portion of the jet where the jet flow interactions with the crossflow. Figure 17 illustrates the streamlines

of the entire channel, which explains the heat transfer behavior caused by jet impingement in the upstream region. The recirculation zone caused by jet-to-jet interaction that appears behind Jet 2, 3 and 4 explains the low heat transfer region as shown in Figure 12. Vortices in front of each jet resulted in lower heat transfer by creating recirculation zones, which is in agreement with the experimental results. Comparing the baseline streamline with the results of the two ideal test cases, Tests 3 and 5 can also be seen in Figure 17. Test 3's heat transfer is significantly enhanced because the jet to jet interactions with jets 2 and 4 are less, as well as crossflow effects. Better mixing has also enhanced the performance of these two jets. For Test 5, the flow field is similar to the baseline case, showing that enhancement for this case seems to be caused by the better impingement, due to increased mass flow rates of jets 1, 2 and 5.

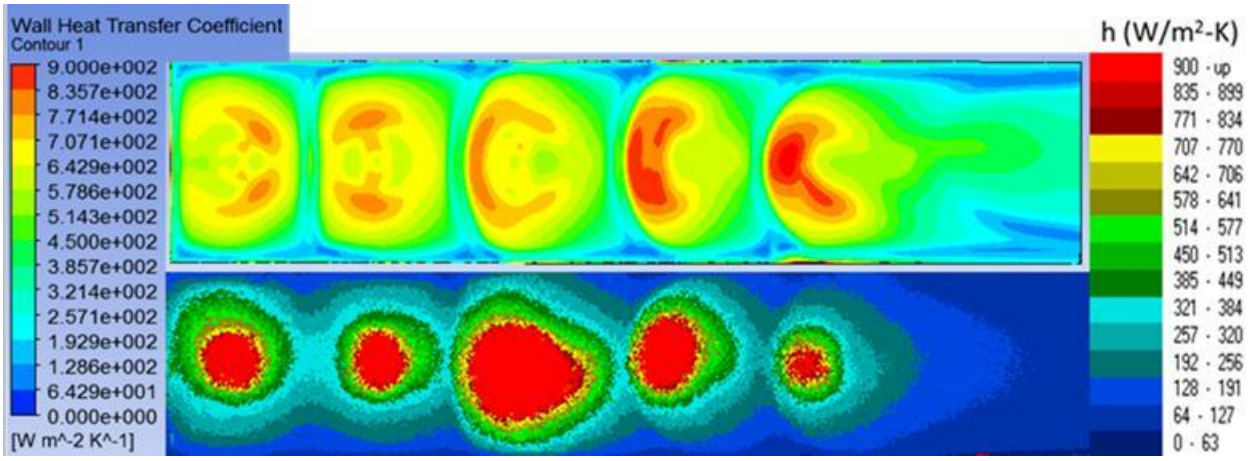

Figure 16. Local Heat Transfer Comparison of Numerical and Experiments Results for Baseline Varying Flow

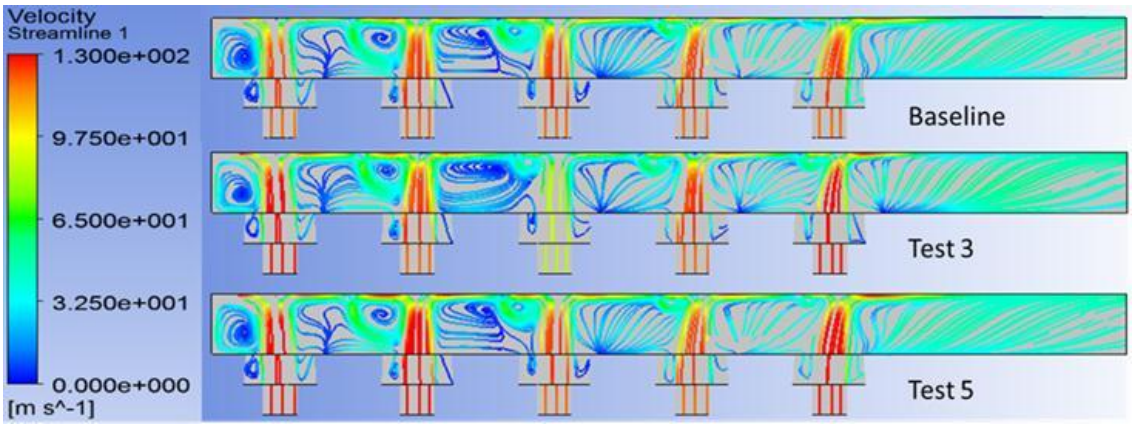

Figure 17. Streamwise Velocity Profile for Baseline and Varying Flow Cases 3 and 5

4.5 KEY FINDINGS

By holding all other parameters constant and having tight control of the flow to each jet, the heat transfer within the jet channel was optimized. With a total variation of ± 2% to the channel Re, an enhancement of 35% was seen when compared to the baseline case. Unfortunately, this type of flow control to each jet is unrealistic for gas turbine applications. In most situations, the jet channel, or an array, will be plenum fed. To fully understand how these varying flow results would translate to the real situation, the varying diameter studies were explored.

5.0 HEAT TRANSFER AND PRESSURE EFFECTS OF VARYING DIAMETER JET PLATES

5.1 LOCAL HEAT TRANSFER COEFFICIENT

Figure 18 shows a comparison of the local heat transfer coefficient, h, using the three different jet plates summarized in Table 2. Because each plate has different diameters, for consistency, the total mass flow rate supplied to the plenum is held constant for each test case. It can be seen for all three cases, that the jet impingement is most profound in the upstream jets, 1 and 2, and decreases in the downstream regions. The crossflow effect can be seen at jets 3, 4 and 5. No deflection can be seen, but the crossflow severely affects the impingement effect of the downstream jets, most notably jet 5. Because the impingement is still preserved in jet 5, the heat transfer coefficient of the downstream regions is then affected by two things: 1) the temperature difference between the crossflow and jet and 2) the flow through the downstream jets is relatively slow compared to the upstream jets. Low flow rate through the downstream jets was confirmed by measuring the pressure of each jet. This was done by inserting pressure taps on the side of the jet plate, and using 6.35 mm (0.25 in) tube and connected to a digital manometer.

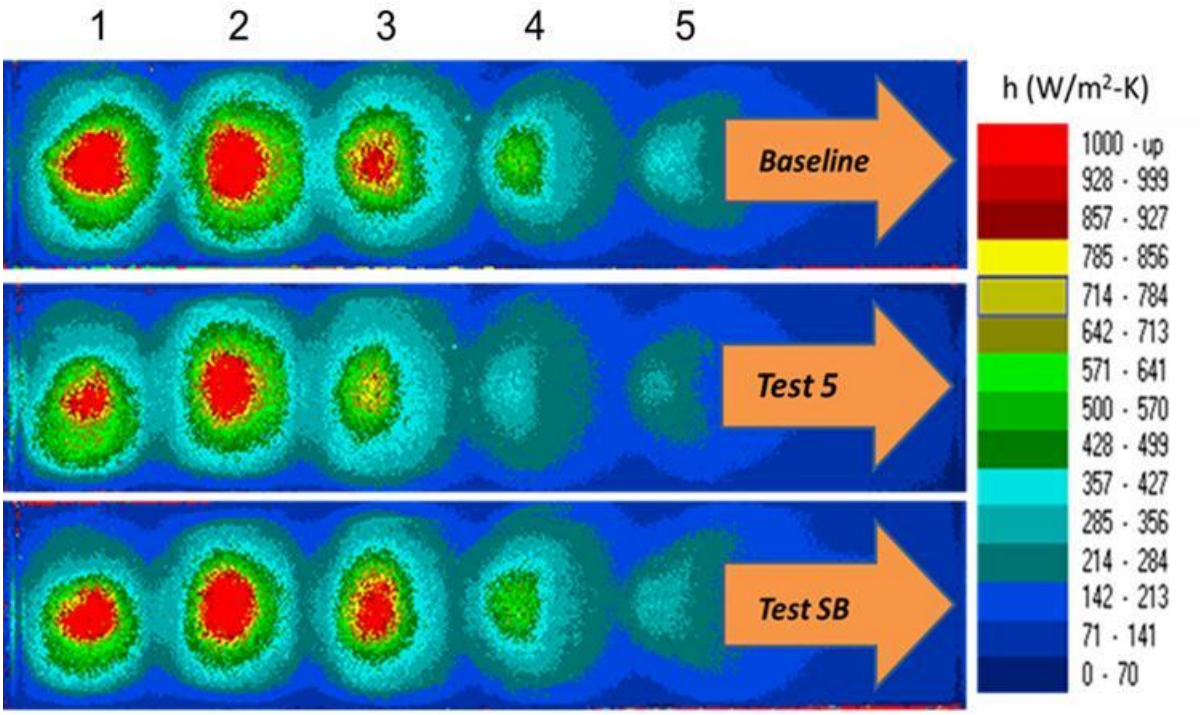

Figure 18. Local Heat Transfer Coefficient for Baseline and Varying Diameter Cases

5.2 SPANWISE AVERAGED HEAT TRANSER

Figure 19 reveals the spanwise average heat transfer of the three jets plates. Again, it remains clear that the highest heat transfer takes place in jets 1 and 2 and then significantly decreases thereafter. Comparing Figure 18 and 19, it is apparent that varying the diameters have an insignificant impact on the heat transfer enhancement. To see a significant difference, one would need to vary the diameters more dramatically, similar to Uysal et al [20]. Figure 20, the total spanwise heat transfer enhancement, clearly shows that the first 3 jets are significantly higher than a smooth channel. The last two jets squander (offset) the effectiveness of the jet channel.

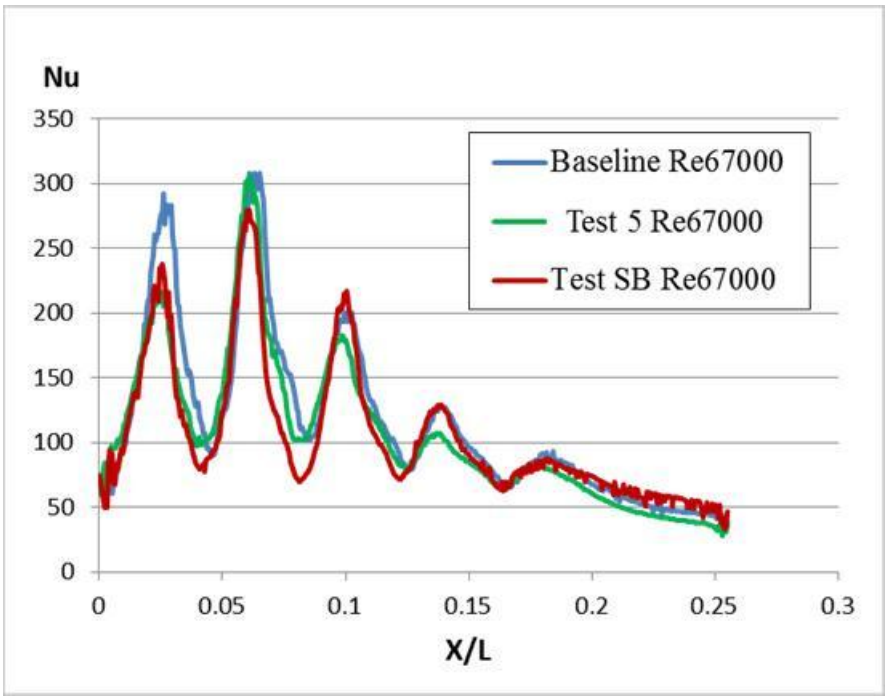

Figure 19. Spanwise Averaged Heat Transfer for Baseline and Varying Diameter Cases

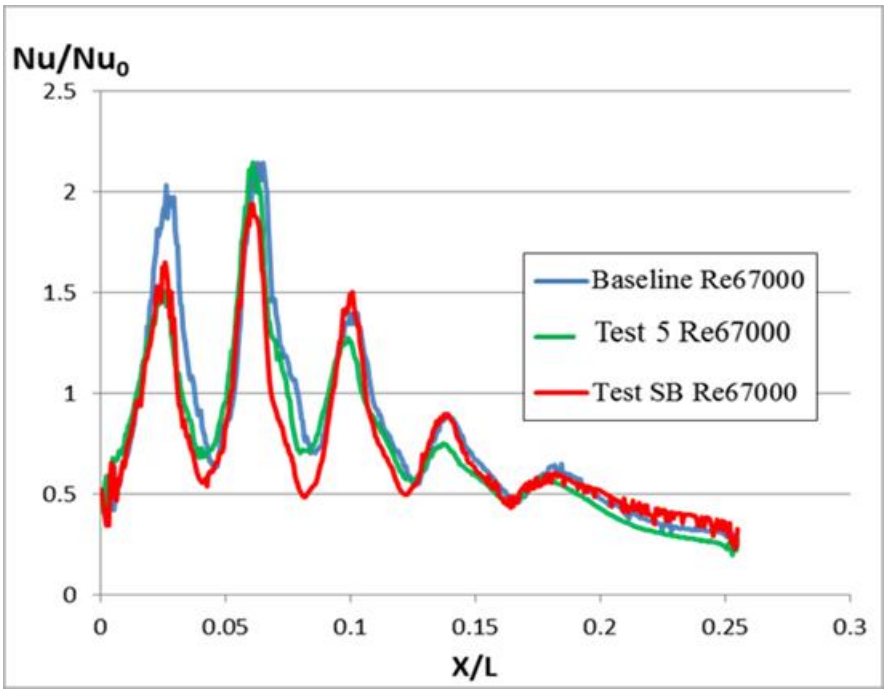

Figure 20. Total Spanwise Averaged Heat Transfer for Baseline andVarying Diameter Cases

5.3 TOTAL HEAT TRANSFER ENHANCEMENT

Figure 21 illustrates the total heat transfer enhancement for the baseline and varying jet diameter arrays normalized by the fully developed smooth channel based on the Dittus-Boelter correlation. Results show that the Test SB, the jet plate with larger downstream jet diameters, has about a 5% heat transfer enhancement over the baseline. To see a greater enhancement, one could decrease the upstream jets further, while also slightly increasing the downstream jets. Test 5 shows a lower enhancement because of the effect of the crossflow on the smaller diameter jet diameters, which have a lower flow rate compared to the upstream jets. In some cases, the total enhancement can be less than one because of the way heat transfer was averaged for Nu_T. The whole target plate domain was used to find an average heat transfer. The low heat transfer areas outside of the impingement location make the enhancement seem less than it really is.

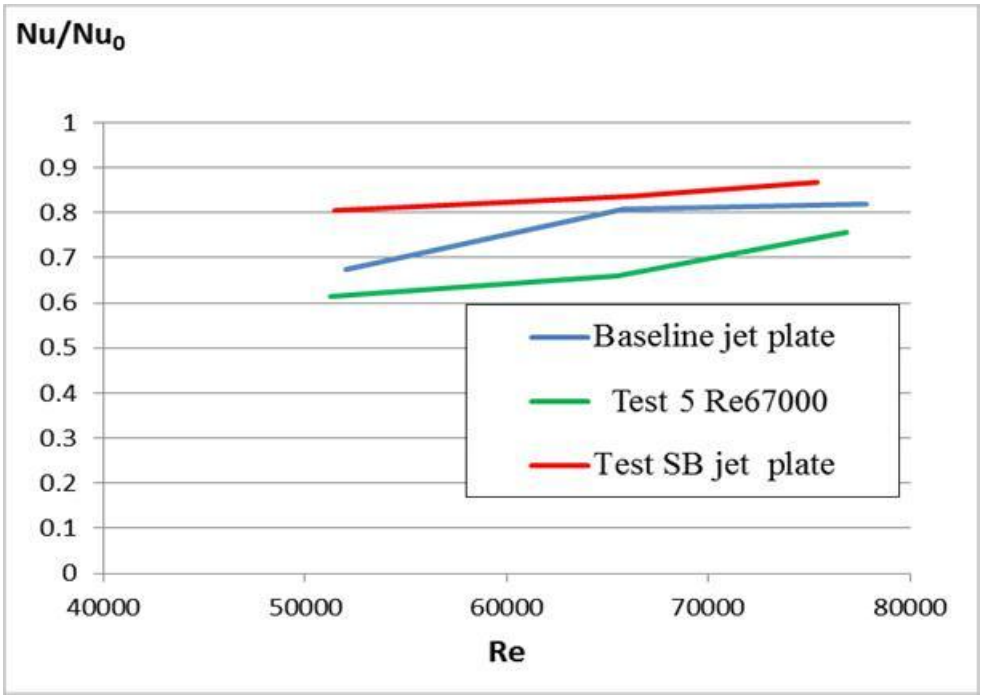

Figure 21. Total Heat Transfer Enhancement for Baseline and Varying Diameter Cases

5.4 PRESSURE LOSS COEFFICIENT

Heat transfer enhancement is always penalized by the pressure loss in the system. The pressure loss characteristics of all jet plates, presented in Figure 22, are based on f/f_0, where f is the friction factor and f_0 is the overall friction factor normalized by the corresponding data for fully developed flow in a smooth channel developed by Petukhov. Dp/dx represents the pressure drop across the jet channel by measuring the static pressure of the plenum compared to atmospheric pressure. All test cases revealed a similar trend in pressure loss as Re increased. The results concluded that the pressure loss in the channel is very much driven by the jet impingement.

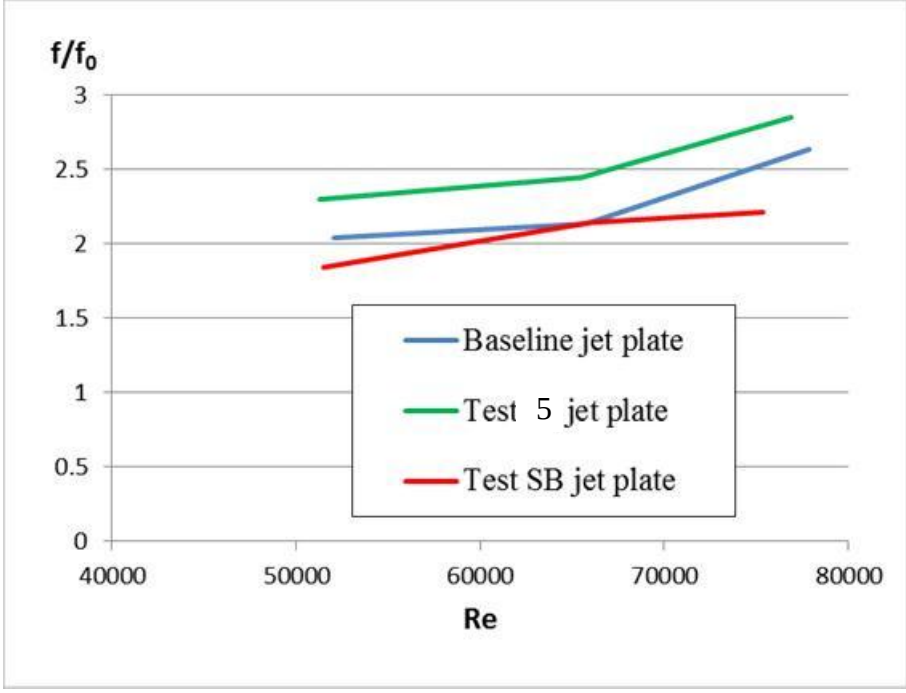

Figure 22. Pressure Loss Comparison of Varying Diameters to Baseline

5.5 NUMERICAL RESULTS

The mesh for the varying diameter cases consists of approximately 2,000,000 elements with the first cell normal to the wall corresponding to a y+ value ≤ 2. Figure 23 shows a comparison of the experimental and numerical local heat transfer coefficients. Overall, the numerical and experimental baseline cases are in agreement, other than the over prediction of the fourth and fifth jets, which is a typical occurrence in jet impingement simulation. As seen in the baseline case from the varying flow study, jets 1 and 2 have higher heat transfer in the stagnation zones, but for jets 3, 4 and 5, heat transfer occurs in the upstream portion of the jet where the jet interacts with the crossflow. When comparing the streamline for the baseline and two varying diameter cases, as seen in Figure 24, it can be seen how differently the flow is being distributed from the plenum to the channel based on the jet diameters. Because the jet diameter of jet 1 is smaller in Test's 5 and SB, the recirculation zone in front of the jet is increased. The other jets are profoundly affects by this and the way the plenum distributes the flow. This makes deflection in the downstream jets is much more prevalent in this cases compared to the varying flow cases.

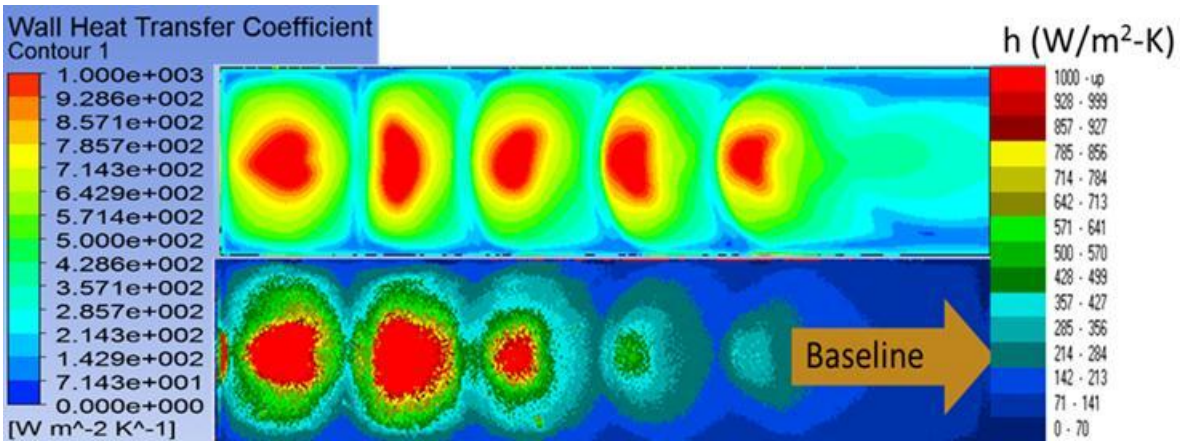

Figure 23. Local Heat Transfer Comparison of Numerical and Experiments Results for Baseline Jet Plate

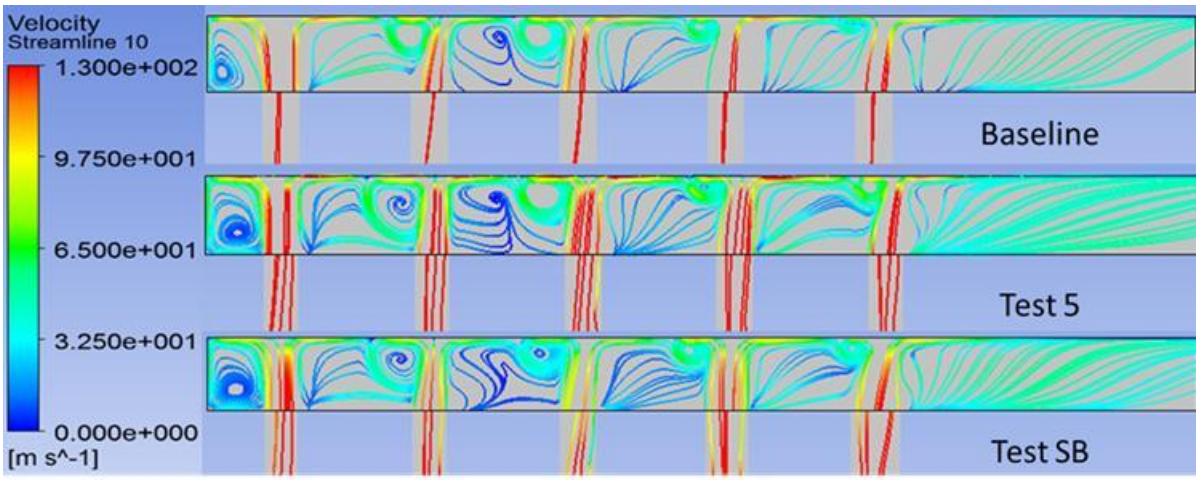

Figure 24. Streamwise Velocity Profile for Baseline and Varying Diameter Cases

5.6 KEY FINDINGS

Although heat transfer enhancement was significantly less than the varying flow cases, some optimism can be taken away from these tests. The nature of flow distribution within the channel does not match well with test 5, which had a small diameter jet at position 5. If partitions were placed within the plenum to help direct and more evenly distribute flow, this jet plate may have performed better than the baseline case. Test SB showed small improvement over the baseline, suggesting that if jet diameters were varied differently, more enhancements could be seen. This could be seen if upstream jets were made even smaller.

6.0 HEAT TRANSFER AND PRESSURE EFFECTS OF STAGGERED AND ANGLED JETS

6.1 LOCAL HEAT TRANSFER COEFFICIENT

Figure 25 shows a comparison of the local heat transfer coefficient, h, of the four different jet plates tested in these experiments as compared to the baseline case. For the baseline case, it can be seen that jet impingement is most profound in the upstream jets, 1 and 2, and decreases in the downstream regions. The crossflow effect becomes more prominent at jets 3, 4 and 5. No deflection can be seen, but the crossflow severely affects the impingement effect of the downstream jets, most notably jet 5. Because the impingement is still present in jet 5, the heat transfer coefficient of the downstream jets are then affected by two dominant factors: 1) the temperature difference between the crossflow and jet and 2) the flow through the downstream jets is relatively slow compared to the upstream jets. Low flow through the downstream jets was confirmed by measuring the pressure of each jet. This was done by inserting pressure taps on the side of the jet plate, and using 6.35 mm (0.25 in) tube and a digital hand held manometer [38]. Based on the pressure distributions, the effects on the heat transfer enhancement for the staggered and staggered angled jets can be better understood. For the staggered cases, as the jet moves closer to the side wall, heat transfer decreases compared to the baseline. As the jet nears the side wall, entrainment greatly affects the impingement. For the staggered angled jets, heat

transfer is enhanced from the baseline case. Due to the jet inclination, the length of the jet until impingement has been lengthened, and it has been shown that for a channel ratio of H/D of 1 to 3, the greater distance to the target plate gives the jet core more time to strengthen [39,40].

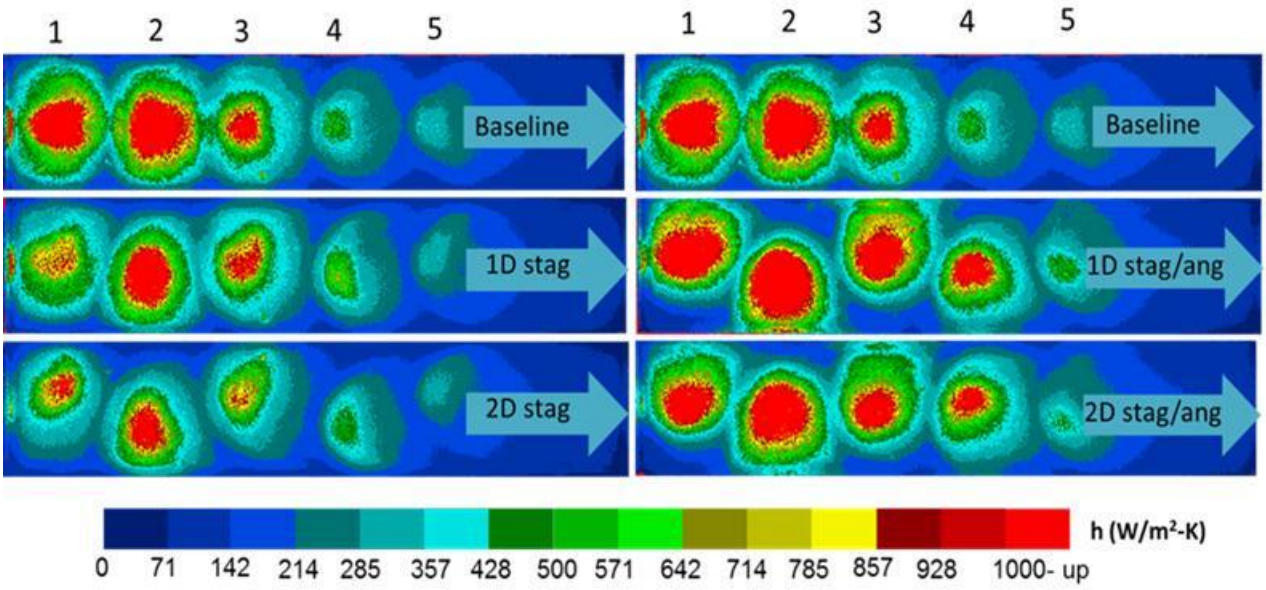

Figure 25. Local Heat Transfer for Baseline, Staggered and Staggered Angled Jets

6.2 SPANWISE AVERAGED HEAT TRANSFER

Figure 26 reveals the spanwise average heat transfer of the staggered jet plates compared to the baseline case. In the 1D and 2D staggered cases, the entrainment effect that occurs near jet 1 has the most effect on the heat transfer enhancement of the array. The crossflow remains the major factor of reduced heat transfer for the downstream jets. In the 2D case, the wall affects the heat transfer more significantly than the 1D case.

Figure 27 shows the spanwise average heat transfer of the staggered angled jet plates compared to the baseline case. For the 1D and 2D staggered angled jets, particularly jets 1 and 2, the enhancement is mostly preserved from the baseline case. The true enhancement comes from the better impingement in jets 3 and 4. As stated above, strengthening the core of the jet helped to improve the impingement throughout the channel, but by changing the impingement location, by staggering and angling the jets, the crossflow affects the channel differently. This will become clearer when examining the numerical results.

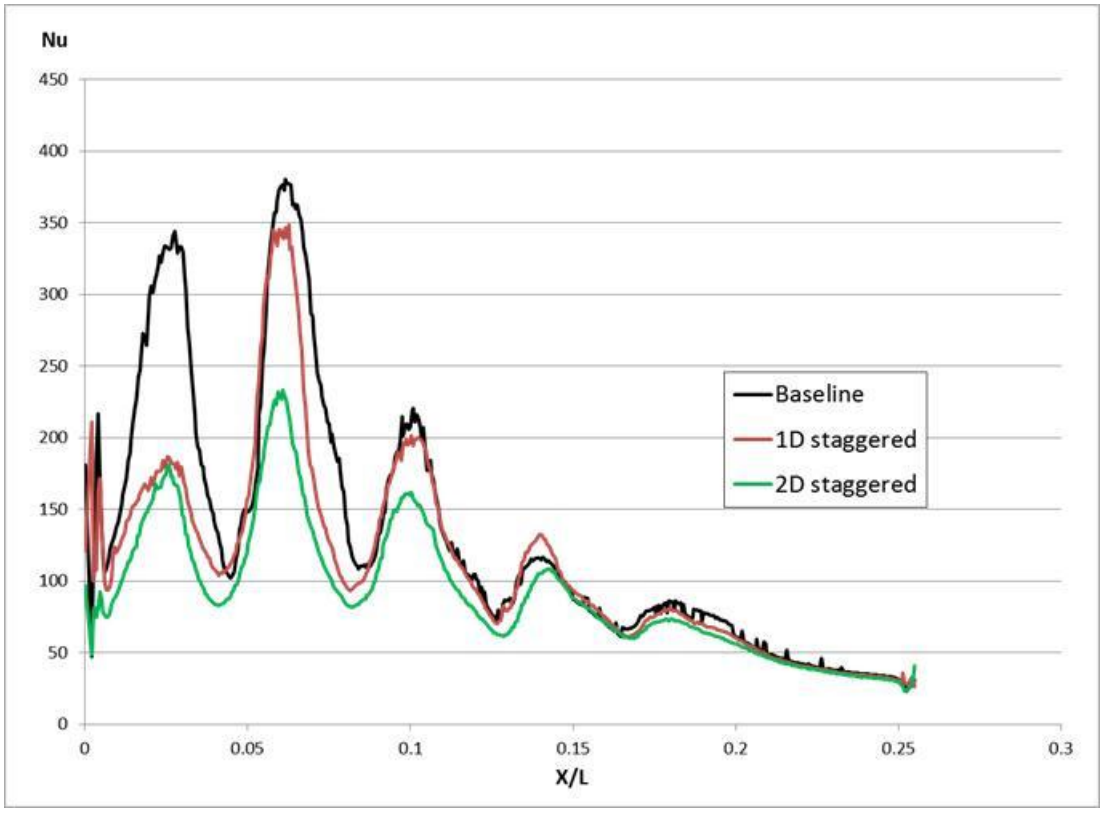

Figure 26. Spanwise Averaged Heat Transfer for Baseline and Staggered Cases

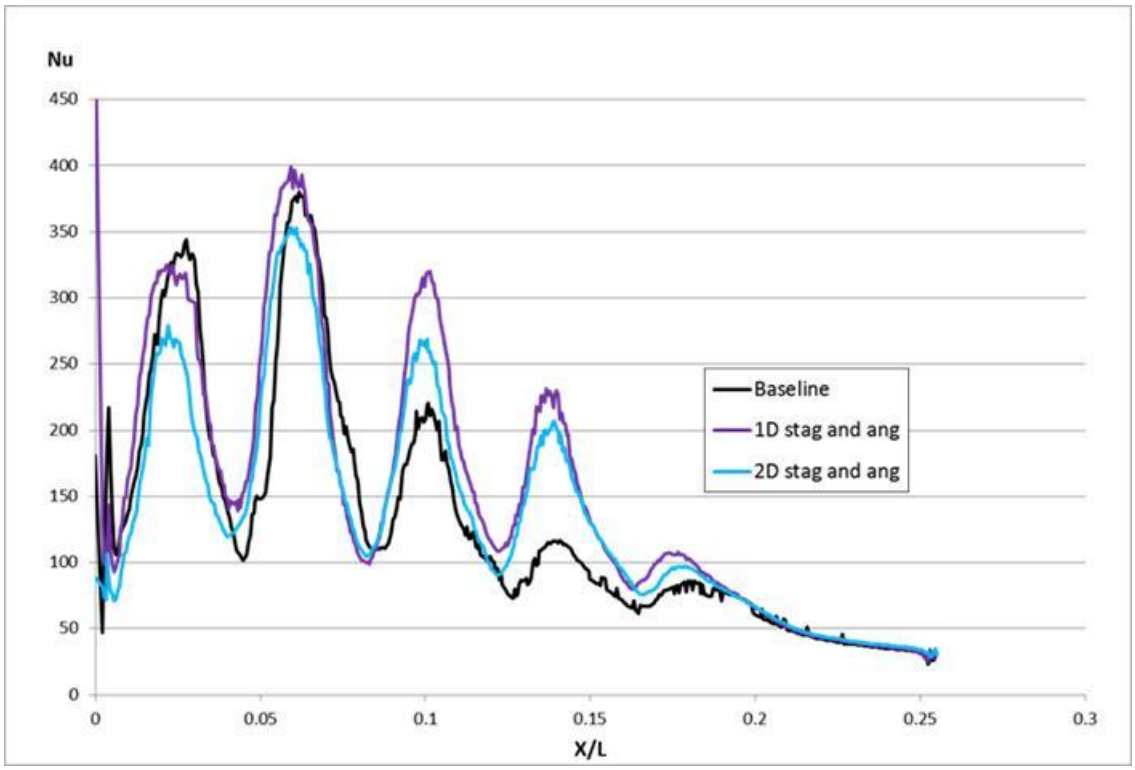

Figure 27. Spanwise Averaged Heat Transfer for Baseline and Staggered Angled Cases

6.3 TOTAL HEAT TRANSFER ENHANCEMENT

Figure 28 illustrates the total heat transfer enhancement for the baseline and four jet arrays normalized by the fully developed smooth channel based on the Dittus-Boelter correlation. Results show that the 1D staggered angled case can improve heat transfer by ≈ 20% over the baseline case. For the 2D staggered angled case, because impingement lies close to that of the inline baseline case, heat transfer in these cases is fairly similar. The staggered cases show lower heat transfer due to the jets being closer to the side walls, making entrain more prevalent. The 1D staggered case could be improved upon by not staggering the first jet. Moving the first jet into the corner significantly affects the overall enhancement of the channel. Also, if the

remaining jets, 2-5, were staggered less, potentially 0.75D, performance could be slightly improved over the baseline. In some cases, the total enhancement can be less than one because of the way heat transfer was averaged for Nu_T. The whole target plate domain was used to find an average heat transfer. The low heat transfer areas outside of the impingement location make the enhancement seem less than it really is.

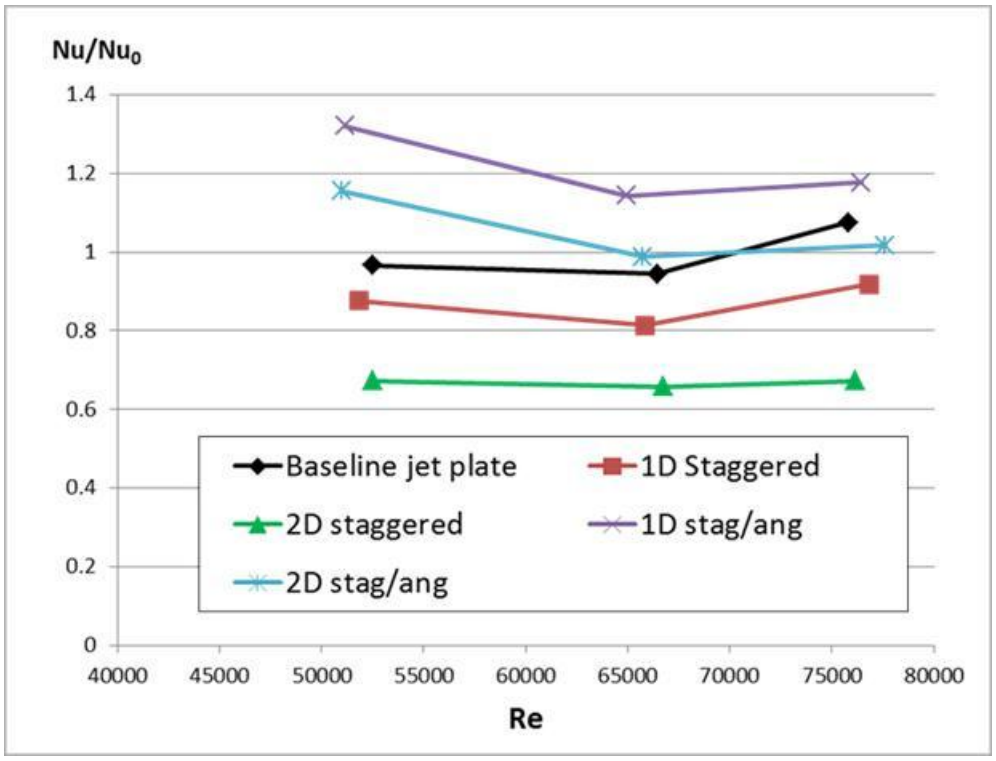

Figure 28. Total Heat Transfer Enhancement of Baseline, Staggered and Staggered Angled Jet Plates

6.4 PRESSURE LOSS COEFFICIENT

The pressure loss characteristics of all jet plates, presented in Figure 29, are based on f/f_0, where f is the friction factor and f_0 is the overall friction factor normalized by the corresponding data

for fully developed flow in a smooth channel developed by Petukhov. Dp/dx represents the pressure drop across the jet channel by measuring the static pressure of the plenum compared to atmospheric pressure. All test cases revealed a similar trend in pressure loss as Re increased. It can be seen that by angling the jets, the pressure drop increases twofold over the baseline case.

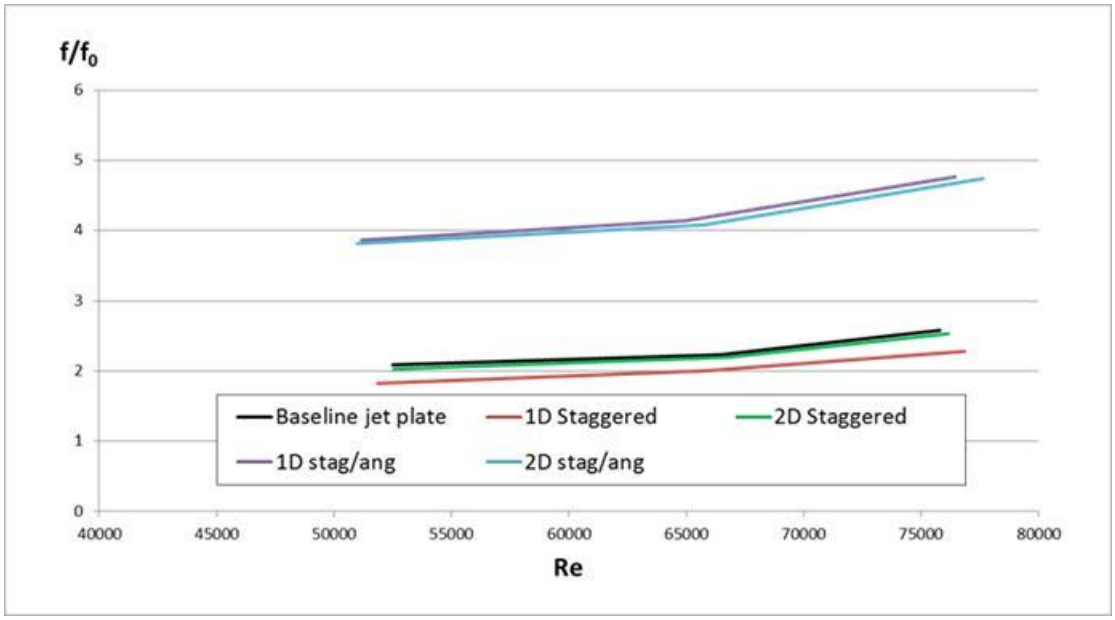

Figure 29. Pressure Loss Due to Staggering and Inclination of Jets

6.5 NUMERICAL RESULTS

The mesh for these cases consists of approximately 2,000,000 elements with the first cell normal to the wall corresponding to a y+ value ≤ 1. Figure 30 shows a comparison of the experimental and numerical local heat transfer coefficients. Local heat transfer is in good agreement for jets 1, 2 and 3. Impingement and turbulence predicted for jets 4 and 5 are over predicted for all cases, but this is a general issue associated with turbulence models predicting jet impingement cases.

To understand the flow characteristics in each case, spanwise and streamwise velocity plots are shown. The baseline case is shown in Figure 31. The vortices to each side of the jet are a significant factor in the overall heat transfer of the jet. Recirculation zones, as well as the jet to jet interactions can entrain flow, lowering the effectiveness of the jet. The same conditions affect the 1D and 2D staggered jets, as well as the 2D staggered angled case. In Figure 32 we can see the characteristics of the 1D staggered angled case. Instead of two side fountains affecting the jet, only one fountain on the side opposite of impingement occurs. This means that flow can impinge and then immediately get swept out by the crossflow. With the crossflow rushing underneath the jet, flow is kept closer to the target surface and can remain in contact longer than any of the other cases. It can also been seen that for the 1D staggered angled case that some additional heat transfer will occur when the flow rolls down the side walls.

Figures 33 and 34 show the mid-plane streamwise velocity plot and the turbulence kinetic energy, respectively. As mentioned previously, Figure 33 confirms that for the angled jets, the jet core has a better chance to develop and strength, providing a more uniform velocity profile. Figure 34 shows that for the angled cases, greater turbulence can be gained near the target surface by changing the angle of impingement. For the 90° cases, the jet will tend to impinge all at once. For the 30° cases, the jet will tend to impinge in sections, causing rolling/tumbling, improving the mixing near the target surface.

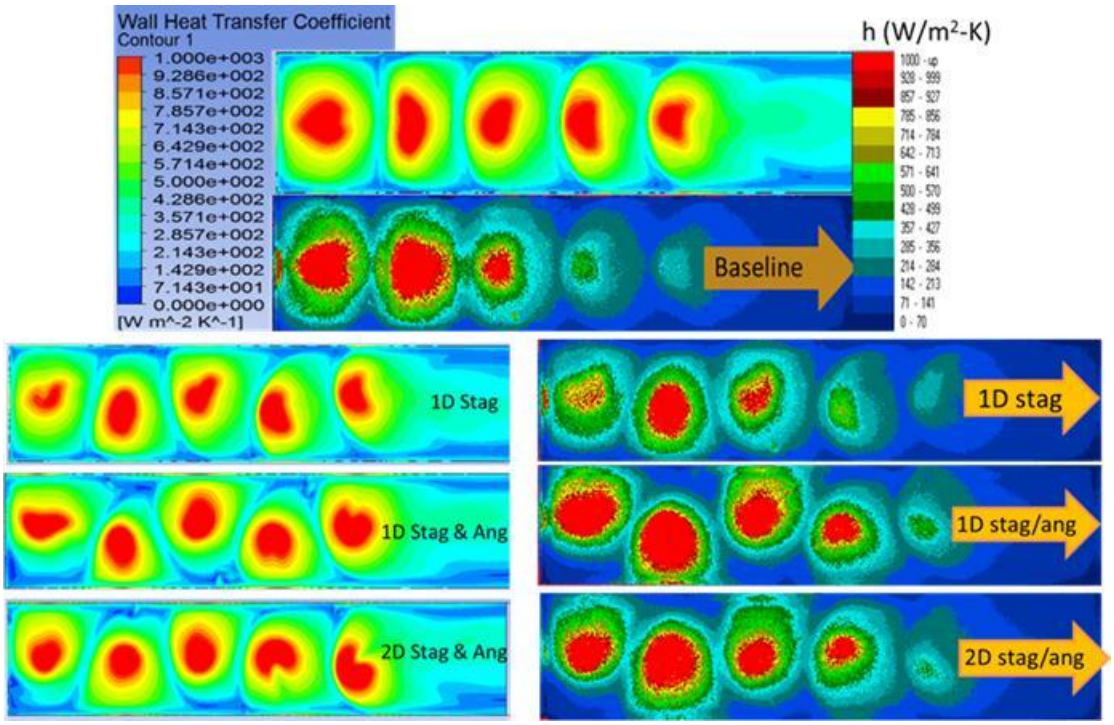

Figure 30. Local Heat Transfer Coefficient of Numerical Baseline, Staggered and Angled Cases Versus Experimental

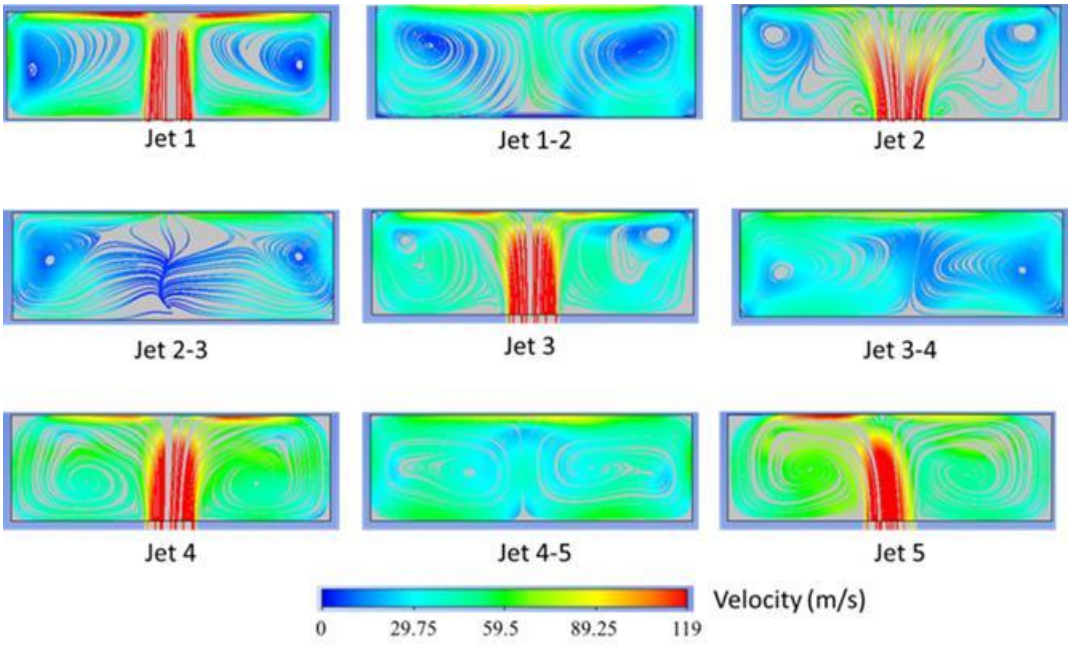

Figure 31. Streamwise Velocity Profile of Plenum Fed Baseline Case

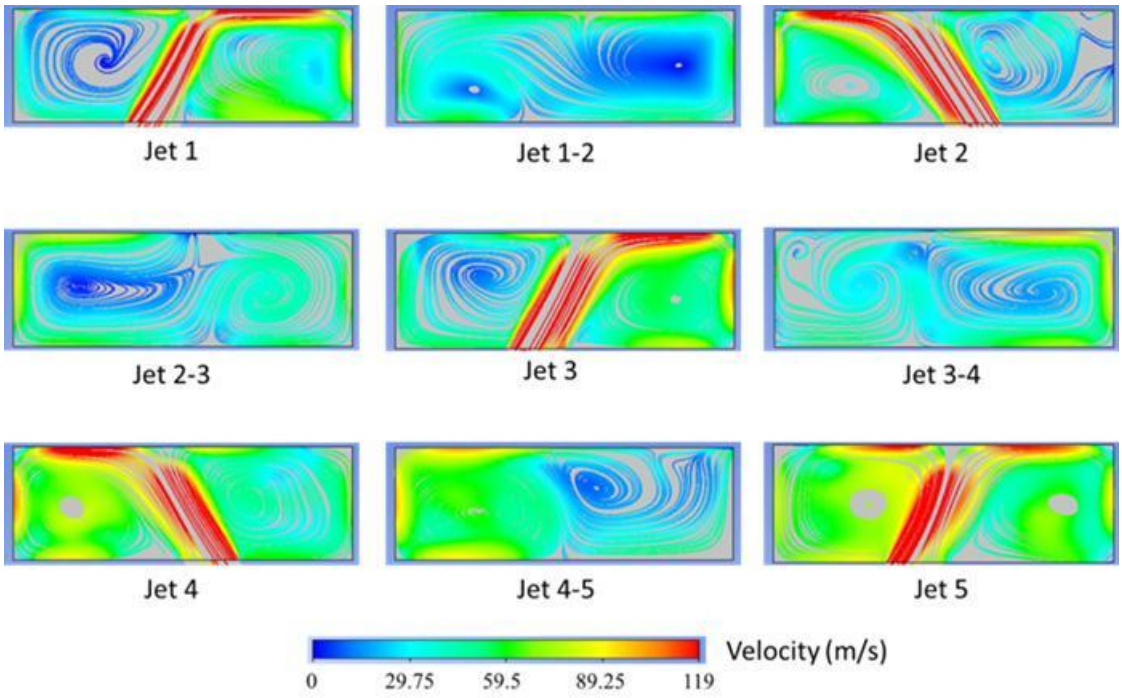

Figure 32. Streamwise Velocity Profile of 1D Staggered Angled Case

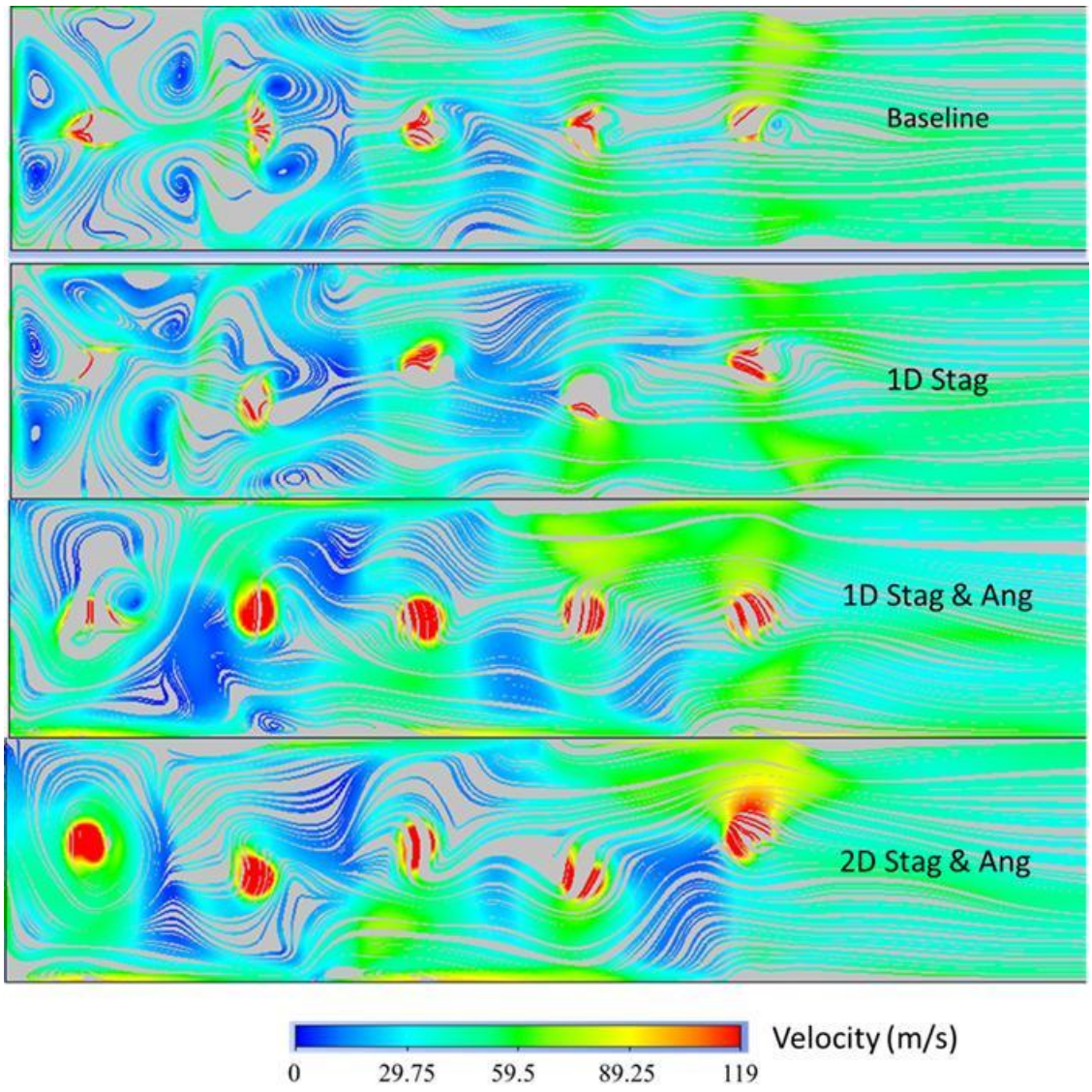

Figure 33. Streamwise Velocity Profile of Jet Channel for Baseline, Staggered and Angled Cases

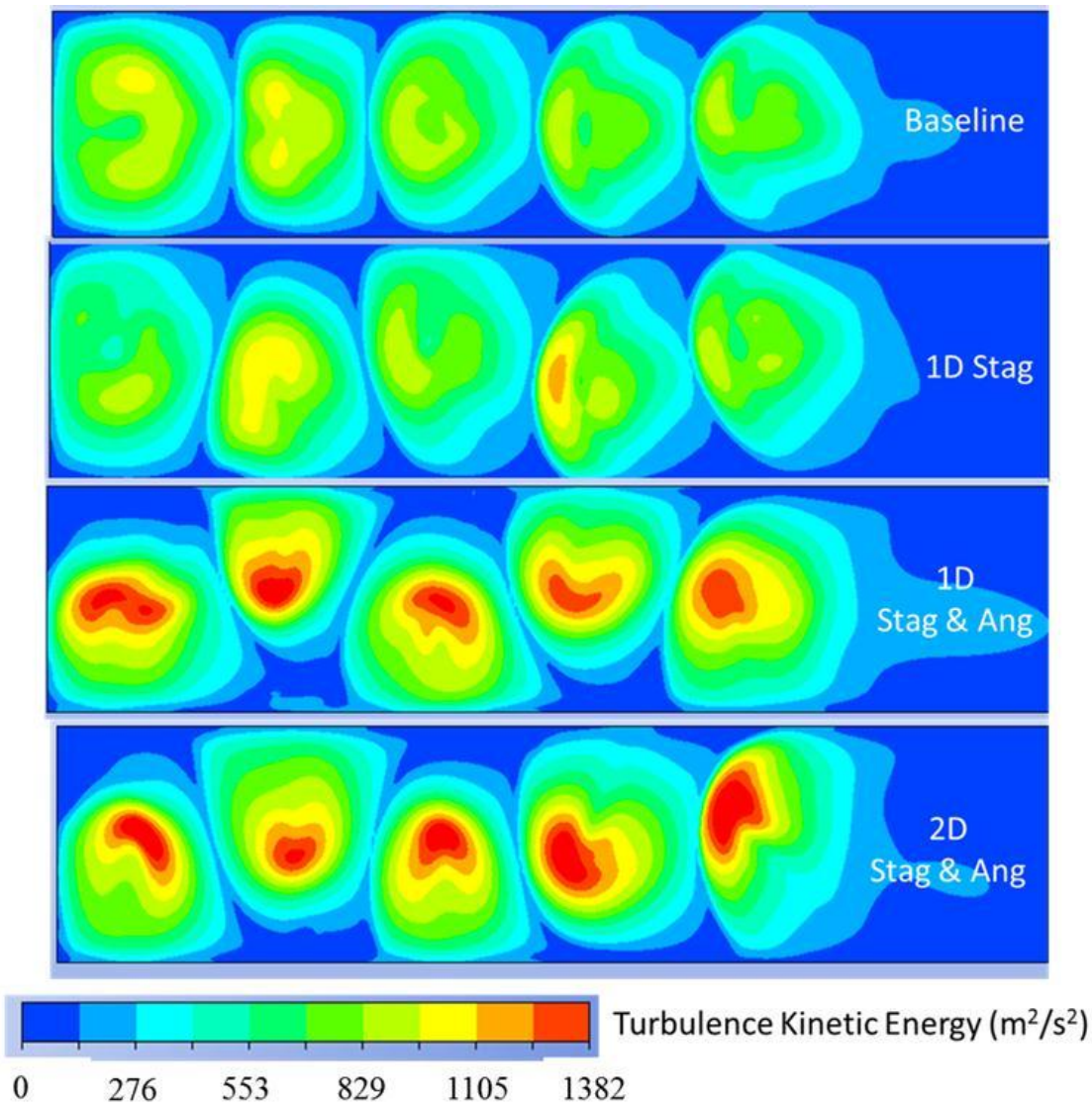

Figure 34. Turbulence Kinetic Energy for Baseline, Staggered and Angled Cases

6.6 KEY FINDINGS

When jets are arranged inline jet to jet interactions and crossflow effects significantly affect the heat transfer of the channel. To minimize these affects, jets can be staggered and/or angled.

Staggering can, however, decrease heat transfer enhancement as it approaches the channel side wall, as seen in these experiments. For this particular channel, had jets be staggered slightly less, < 1D, improvement over the baseline may have been seen. Even for the 1D staggered case studied, had the first jet not been staggered, heat transfer performance would have been fairly similar to the baseline case, which is evident from Figure 26.

For the angled cases, most previous studies angled jets in the streamwise position, either positioned upstream or downstream [21,22]. These studies found that angled impingement offered fewer enhancements over the baseline. Flow was either consumed by the crossflow (angled upstream), losing the full effect of the impingement, or flow would be washed away (angled downstream). By staggering (as not to impinge too close to the channel side walls) and angling the jets in the spanwise direction, a 20% heat transfer enhancement was observed. This was due to the jet core having more time to develop and the angle of impingement causing better mixing. The downfall of angling the jets is the pressure loss, twofold increase compared to the baseline as the angled jet plate is more restrictive, requiring more pressure to force flow through the jet plate.

7.0 HEAT TRANSFER AND PRESSURE EFFECTS OF JET CHANNEL WITH SURFACE ROUGHNESS

7.1 LOCAL HEAT TRANSFER COEFFICIENT

Figure 35 shows the local heat transfer coefficient of the baseline and three different target plates. As with the jet plates, the performance remains better in the upstream than in the downstream, but it can be seen with the presence of surface roughness, the downstream areas can be enhanced. The impingement zones are largely preserved in all test cases. In the upstream regions, heat transfer remains largely dominated by impingement. This trend is reversed as the flow propagates downstream, where heat transfer is higher near the ribs and lower in the impingement areas. The baseline case and 90 degree ribs have comparable heat transfer distribution, except that the rib has higher heat transfer than that of the neighboring region. The heat transfer distribution for chevrons and X-shaped ribs appear to mimic the shape of the ribs as flow tends to travel along the rib at the outer region of the impingement zones.

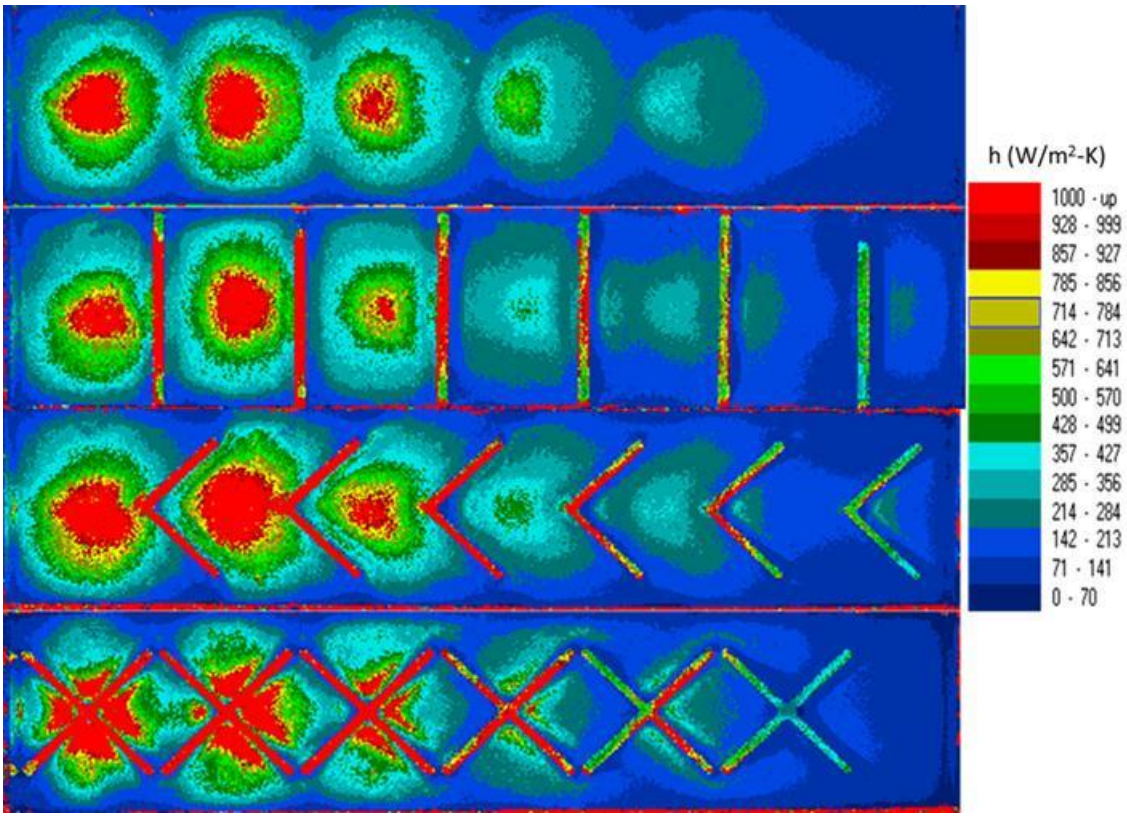

Figure 35. Local Heat Transfer Coefficient for Baseline and Different Surface Roughness Geometries

7.2 SPANWISE AVERAGED HEAT TRANSFER

A better idea of the general enhancement can be seen by the spanwise average heat transfer shown in Figure 36. 90 degree ribs in the presence of jet impingement actually decreases heat transfer in the upstream regions, jet 1 and 2, and slightly increases the downstream regions. This agrees with the findings of Annerfeldt et al. [26]. However, the results also revealed that the 90^{o} ribs are proven to enhanced the local heat transfer effectively, which is up to several folds higher than that of other test cases. Such a high non-uniform spatial distribution of heat transfer may ultimately create a hot spot in the domain. In the upstream regions it would appear that the entrainment of the crossflow caused by the ribs, as compared to the baseline where crossflow can

exit freely, is affecting the heat transfer of the jet impingement. The low temperature difference between crossflow and jet is hindering the heat transfer enhancement. The ribs themselves are the only actual performance enhancement in this case. In contrast, the performance of the upstream regions is preserved in the presence of chevrons and X-shaped ribs. The chevrons show a certain level of enhancement for jets 1 and 2, but then decreases severely in the downstream region. The chevron ribs themselves, as with the 90 degree ribs, are the most beneficial enhancement.

The X-shaped ribs show the best performance of all cases, both in the upstream and downstream regions. At all 5 jets, enhancement is best above and below the impingement zone and immediately downstream of each jet.

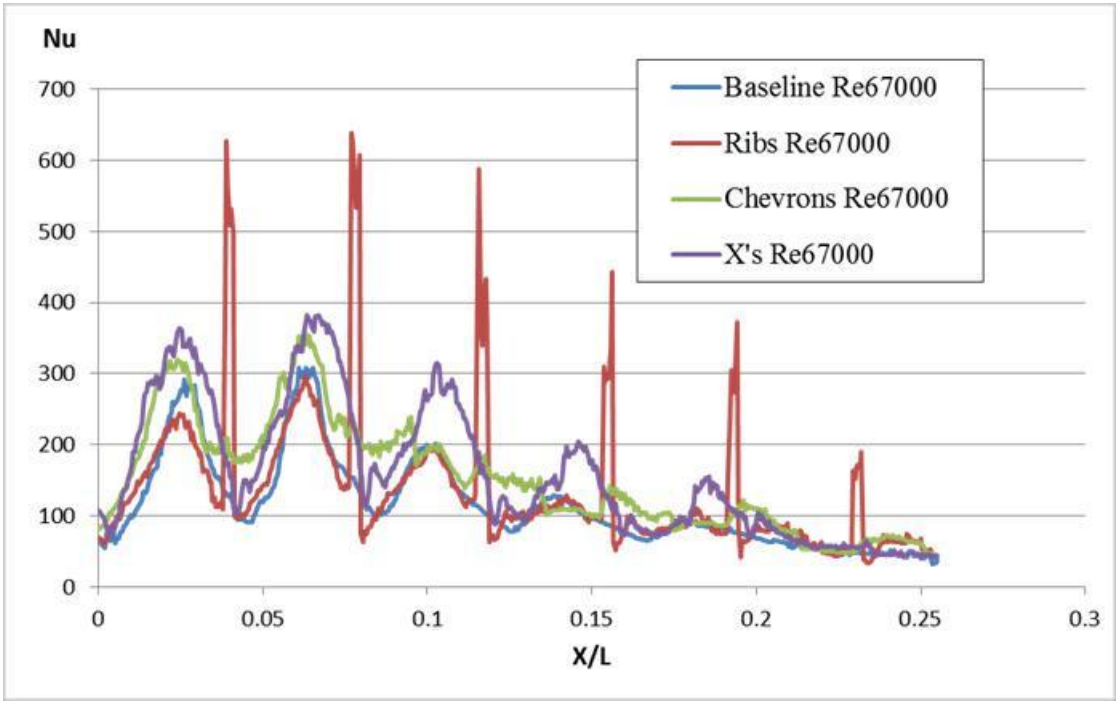

Figure 36. Spanwise Averaged Heat Transfer of Baseline and Surface Roughness Geometries

7.3 TOTAL HEAT TRANSFER ENHANCEMENT

Figure 37 illustrates the total heat transfer enhancement for the baseline and varying jet diameter arrays normalized by the fully developed smooth channel based on the Dittus-Boelter correlation. The results in Figure 16 agree with that of Annerfeldt et al. [26], where it was found that Nu could be enhanced by a factor of 1-1.3. In some cases, the total enhancement can be less than one because of the way heat transfer was averaged for Nu_T. The whole target plate domain was used to find an average heat transfer. The low heat transfer areas outside of the impingement location make the enhancement seem less than it really is.

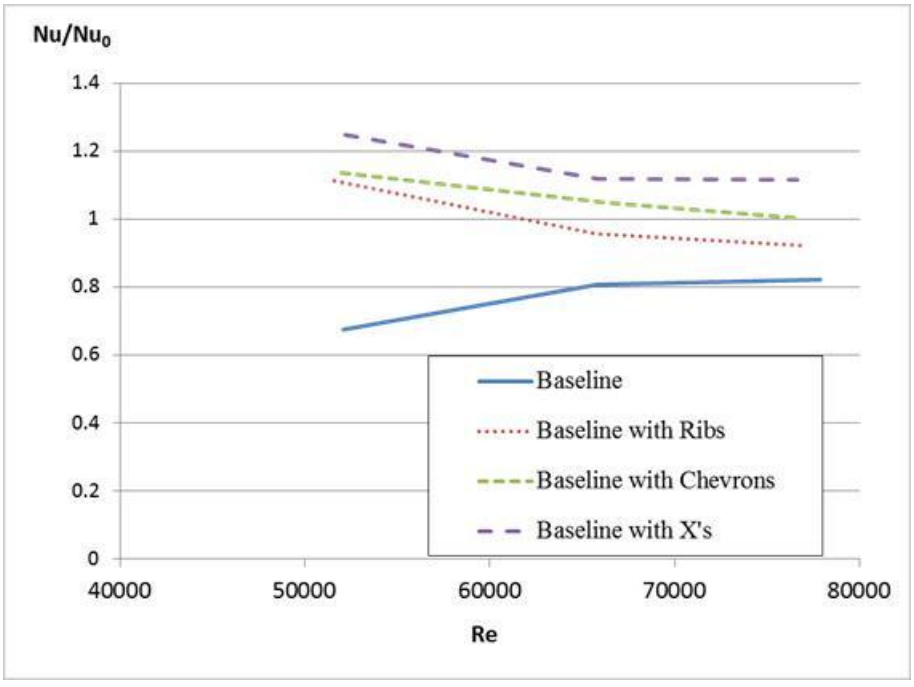

Figure 37. Total Heat Transfer Enhancement of Surface Roughness Geometries in Jet Channel

7.4 PRESSURE LOSS COEFFICIENT

The pressure loss characteristics of all surface roughened target plates presented in Figure 38 are based on f/f_0, where f is the friction factor and f_0 is the overall friction factor normalized by the corresponding data for fully developed flow in a smooth channel developed by Petukhov. Dp/dx represents the pressure drop across the jet channel by measuring the static pressure of the plenum compared to atmospheric pressure. All test cases revealed a similar trend in pressure loss as Re increased. Figure 38 shows that the addition of surface features on the target plate does not greatly affect the pressure drop of the channel. The results concluded that the pressure loss in the channel is very much driven by the jet impingement and from the restriction of flow through the jet plates.

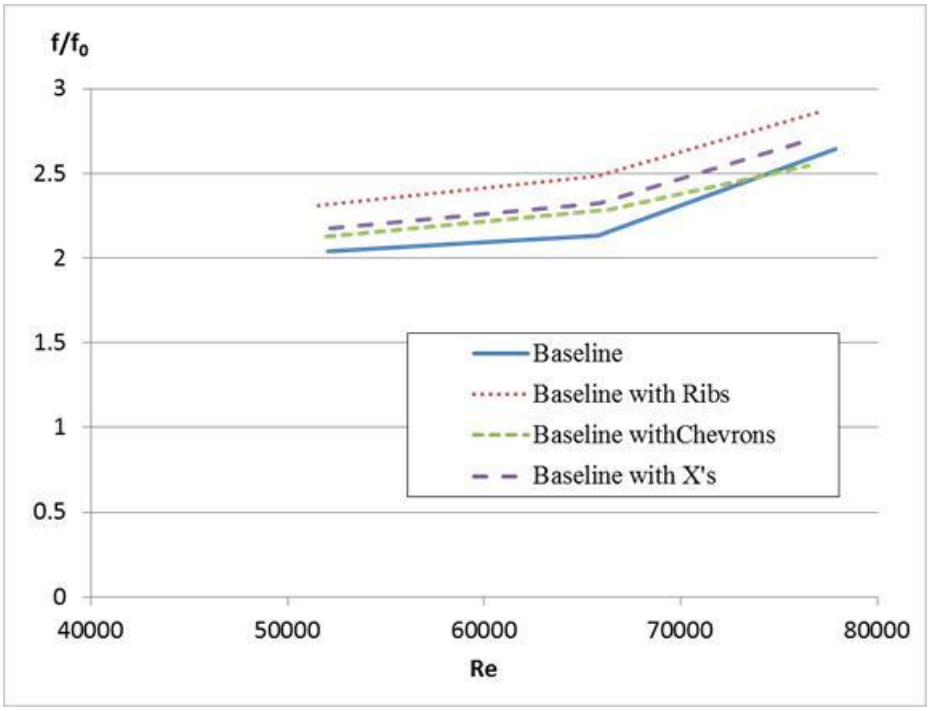

Figure 38. Pressure Loss of Jet Channel with Different Surface Roughness Geometries

7.5 KEY FINDINGS

Jet impingement heat transfer is quite effective, the best of all cooling designs in fact, but it can become non-uniform do to crossflow effects. Hence the use of surface roughness in areas of low heat transfer, specifically in the downstream regions were heat transfer becomes strictly convective and less impingement occurs. 90° ribs should not be used in the upstream regions due to increased recirculation zones that affect the heat transfer of the jet impingement. Broken ribs could perform better in the upstream areas. The chevron and X-shaped ribs, however, do help to increase heat transfer in the impingement stagnation areas. Chevrons only help in jets 1 and 2, but an increase can be seen in all jets for the X-shaped ribs.

8.0 HEAT TRANSFER AND PRESSURE EFFECTS OF STAINLESS STEEL JET COUPONS WITH VARYING H/D

8.1 TOTAL HEAT TRANSFER ENHANCEMENT

Figure 39 illustrates the total heat transfer enhancement for the two stainless steel coupons normalized by the fully developed smooth channel based on the Dittus-Boelter correlation. Results show that as Re increases the 2 mm high channel offers better heat transfer than the 1 mm high channel. These results correlate well with those provided in the literature [10,13,17,18,39]. There are two main dominating factors controlling the heat transfer in the coupons: 1) development of jet core and 2) crossflow effects in downstream regions. For the lower Re, it's clear that the closer the jets are to the hot surface the better the performance. As Re increases and flow is more turbulent, a short channel offers less space for the jet core to develop. This is why the 2 mm high channel performs better at high Re.

For both channel heights, it is seen that both perform much worse at higher Re. Because the channels are very restrictive, crossflow will severely affect the downstream jets and present the potential of plugging.

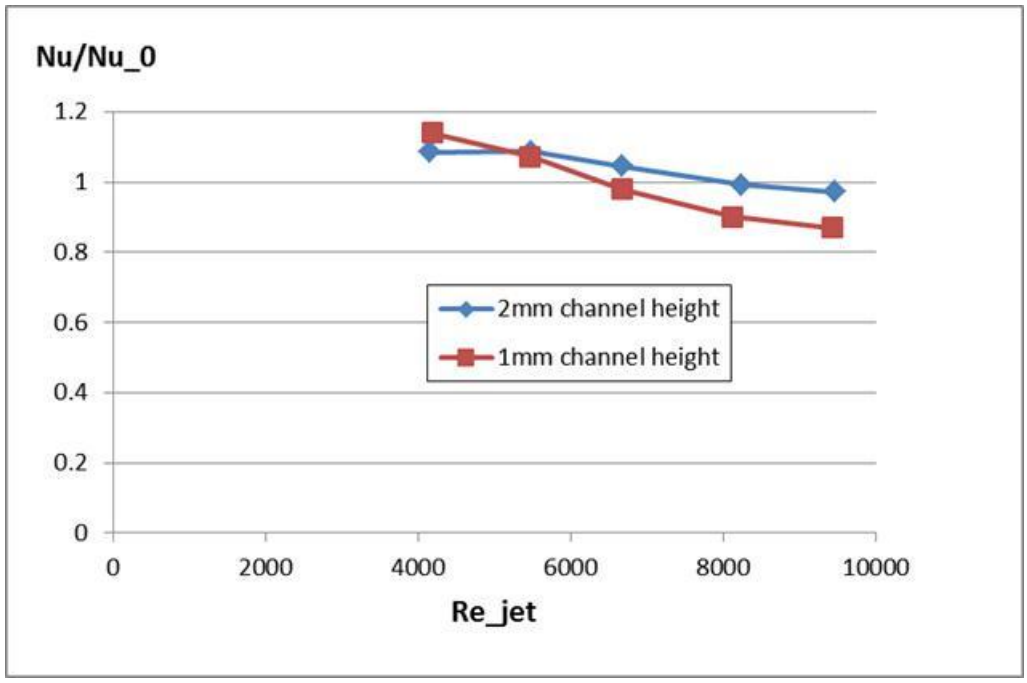

Figure 39. Total Heat Transfer Enhancement of SS Coupons with H/D of 1 and 2

8.2 PRESSURE LOSS COEFFICIENT

The pressure loss characteristics of the two coupons, presented in Figure 40, are based on f/f_0, where f is the friction factor and f_0 is the overall friction factor normalized by the corresponding data for fully developed flow in a smooth channel developed by Petukhov. Dp/dx represents the pressure drop across the jet coupons by measuring the static pressure of the plenum compared to atmospheric pressure. Both coupons revealed a similar trend in pressure loss as Re increased. It can be seen that a difference of 1 mm in height can increase pressure drop by roughly 1.5.

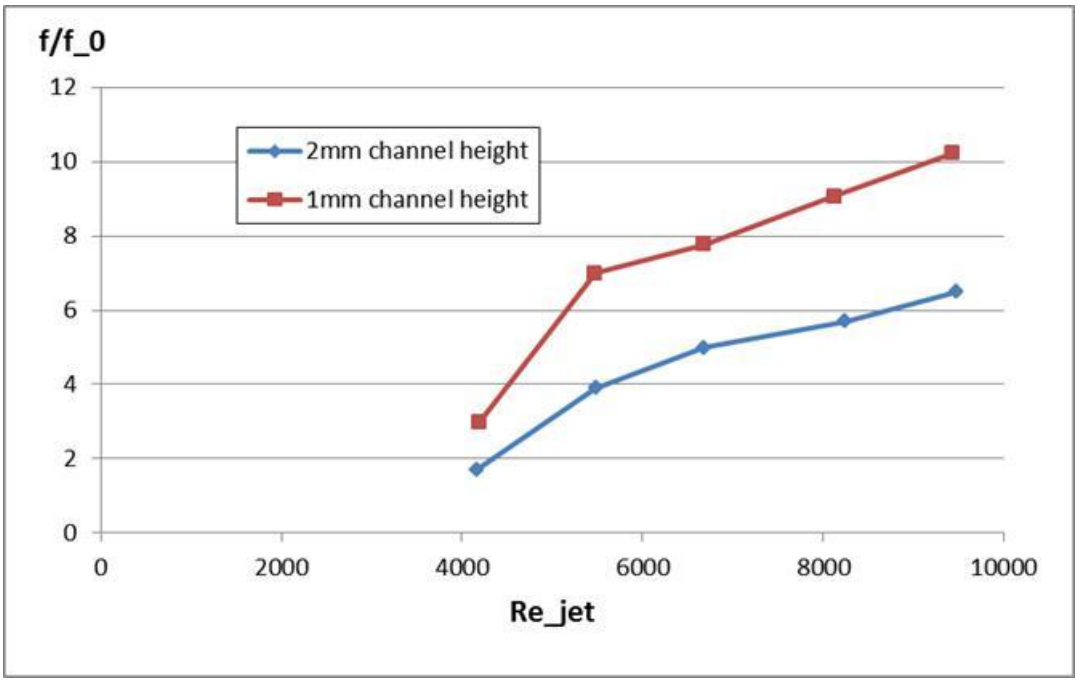

Figure 40. Pressure Loss of Jet Coupons with H/D of 1 and 2

8.3 KEY FINDINGS

The jet coupons were scaled down to be able to validate what was perceived at the scaled up level. As is with most test cases, a baseline is needed to compare experimental results to and these coupons acted as such. Expecting the 2 mm channel to have a better performance, as literature predicted, is exactly what we found. Also, the 1 mm channel, which had more confined jet channels, experienced higher pressure loss as expected.

9.0 CONCLUSIONS AND FUTURE WORK

9.1 CONCLUSIONS

The present study describes a detailed experimental/numerical analysis of jet impingement cooling for gas turbine airfoils, specifically double wall cooled blades. This investigation looked at several different varying flow rates, while maintaining constant jet diameter and channel dimensions. Experimental results showed that by varying the flow to the jet channel by ±2%, that the total heat transfer enhancement could be up to 35% better than the baseline case where all jets had identical flow. It was found that the center most jet, Jet 3, played the greatest role in optimizing the jet flow. By setting the other four jets at relatively constant flow rates across all tests, we were able to decrease Jet 3 to found the flow rate that would help to optimize the heat transfer of the entire channel. The results from these experiments were used to fashion a jet plate with varying diameters to see how the results would compare.

Ultimately, because the varying jet plates used a plenum to feed the flow, which made it a more realistic case, flow to the jets was not uniform, causing the crossflow to be much more prominent. To use the results from this current study to build an array with varying diameters, one would need to partition the plenum in such a way that the flow was properly distributed.

To build upon the previous studies, it was apparent that to improve upon the inline baseline cases, the jet array would need to be altered. Results for the inline jet array (baseline

case) show jet to jet affects can affect the upstream jets, while jets in the downstream region are heavily affected by the crossflow. Staggering and angling the jets were investigated to optimize the jet impingement in the channel. Staggering alone, as seen in the 1D and 2D cases, was not enough to enhance heat transfer in the channel. For these cases, entrainment caused from side wall interactions actually decreased performance. The best case was seen in the 1D staggered angled case were total heat transfer performance was increased over the baseline by ≈ 20%. Although there is a penalty for the increased pressure drop, the staggered angled case can still be a viable option to increase jet impingement heat transfer.

Additionally, surface features on the jet channel target plate were used to optimize the inline jet array (baseline). Results of the surface roughened target plates show that when 90 degree ribs are present between jets, the jet impingement heat transfer enhancement is decreased. Overall performance of the 90 degree ribs shows decreased heat transfer in the upstream jets, but increased heat transfer in the downstream regions. The ribs themselves offer the best enhancement. In the case of the chevrons, upstream jet impingement is preserved, but there is only a slight increase in the downstream regions. The X's provided the best enhancement, both in terms of preserving the jet impingement in the upstream regions and increasing heat transfer in the downstream regions, most notably in the impingement zone of jets 4 and 5.

Ultimately, scaling the experimental models down is critical to the turbine designer to understand how the cooling features behave at a realistic level. Using the stainless steel jet coupons helped to put reported results into perspective, and those results were achieved using this test setup. However, due to the manufacturing price of the coupons, it is critical to consider the appropriate/optimum scaled up model to scale down.

By using numerical analysis in conjunction with the experimental tests, we were able to back up the heat transfer results we saw and were able to better understand how the flow characteristics of the jet array played into those factors.

9.2 FUTURE WORK

A sizable amount of work was accomplished under this project, but a lot remains available to approve upon. Further investigations into the plenum design, staggered and staggered angled jet plates, and additional coupon testing could help to strength the results discussed above.

1. In most realistic cases, a plenum will feed an entire jet array or jet channels. Understanding how the plenum distributes flow and how to optimize flow is critical to the uniformity of the heat transfer supplied by jet impingement. If more flow could be diverted to the downstream regions, this may be possible.
2. There is room to further improve upon the enhancement of staggered and staggered angle jets. For only staggered jets, if staggering was less than 1 and the first jet, the jet in the most upstream position, is left centered in the channel (no staggering), enhancement over the baseline may be seen, and with no pressure loss. For the staggered angled jets, both the staggering distance and degree of angle could be further investigated to see if the current enhancement (from the 1D staggered and angled case) can be outperformed. Another important study related to the staggered angled cases is to explore the S/D. As stated above, the typical S/D is between 4-6. With spanwise angled jets, this distance could shrink and improve uniformity within the channel.

3. Surface roughness could help to further increase the enhancement offered by staggering and inclination. Because low heat transfer will occur outside of the stagnation zones, surface feature could be used in those areas to increase mixing.
4. Once the above are completed, more coupons could be explored. To improve upon the original coupon testing, it would be good to perform IR tests to see how the surface temperatures increase along the jet channel due to crossflow effects. As seen in the scaled up measurements, performance weakened after the third jet. If this is just as significant at the scaled down level, micro channels could be shortened to the appropriate amount of jets and could be conjoined with film cooling holes. This way, more channels could be positioned in line and all would provide great cooling abilities.

BIBLIOGRAPHY

[1] Lakshminarayana, B., 1996, "Fluid Dynamics and Heat Transfer of Turbomachinery", John Wiley and Sons, Inc.

[2] Lee, E., Wright, L.M., and Han, J.C., 2003, "Heat Transfer in Rotating Rectangular Channels (AR=4:1) with V-Shaped and Angled Rib Turbulators with and without Gaps,"ASME Paper No. GT2003-38900.

[3] Han, J.-C., Dutta, S., and Ekkad, S., 2000, Gas Turbine Heat Transfer and Cooling Technology, Taylor and Francis, New York.

[4] Florschuetz, L. W., Metzger, D. E., and Su, C. C., 1984, "Heat transfer characteristics for jet array impingement with initial crossflow", J. Heat Transfer 106, 34–41.

[5] Lutum, E., Semmler, K. and von Wolfersdorf, J., "Cooled Blade for a Gas Turbine, US Patent, US6379118 B2, US Patent, 2002.

[6] Bunker, R.S., 2013, "Gas Turbine Cooling: Moving From Macro To Micro Cooling", ASME Turbo Expo, GT2013-94277

[7] Chyu, M.K. and Alvin, M.A., "Turbine airfoil aerothermal characteristics in future coal–gas-based power generation systems", Heat Transfer Res. 41 (7) (2010) 737–752.

[8] Bunker, R.S. and Wallace, T.T., 1994, "Turbine Airfoil with Double Shell Outer Wall," US Patent 5,328,331.

[9] Sellers, R.R., Soechting, F.O., Huber, F.W. and Auxier, T.A., 1998, "Cooled Blades For A Gas Turbine Enginer," US Patent 5,720,431

[10] Weigand, B., and Spring, S., 2011, "Multiple Jet Impingement—A Review", Heat Transfer Res., 42(2), pp. 101–142.

[11] Downs, S.J. and James, E.H. 1987, "Jet Impingement Heat Transfer – A Literature Survey", ASME National Heat Transfer Conference, Pittsburgh, Pennsylvania, Aug. 9-12, 87-HT-35

[12] Jambunathan, K. and Button, B.L., 1994, "Jet-Impingement Heat Transfer: A Bibliography 1986-1991", Previews of Heat and Mass Transfer, Vol.20, No.5, pp.385-413

[13] Han, B. and Goldstein, R., 2000, "Jet-Impingement Heat Transfer in Gas Turbine Systems", Annals of the New York Academy of Sciences", Vol. 934, No.1, pp.147-161

[14] Martin, H., 1979, "Heat and Mass Transfer Between Impinging Gas Jets and Solid Surfaces, Advances in Heat Transfer, Academic Press, New York, Vol. 13, pp. 1-60

[15] Livingood, J. N. B., and Hrycak, P., 1973, "Impingement Heat Transfer from Turbulent Air Jets to Flat Plates-A Literature Survey", NASA, Lewis Research Center

[16] Obot, N.T. and Trabold, T.A., 1987, "Impingement Heat Transfer within Arrays of Circular Jets: Part 1- Effects of Minimum, Intermediate, and Complete Crossflow for Small and Large Spacings", ASME Journal of Heat Transfer, Vol. 109, pp.872-879

[17] Hollworth, B.R. and Cole, G.H., 1987, "Heat Transfer to Arrays of Impinging Jets in a Crossflow", Journal of Turbomachinery, Vol. 109, pp.564-571

[18] Goldstein, R. and Seol, W., 1991, "Heat Transfer to a Row of Impinging Circular Air Jets including the Effect of Entrainment", Int. Journal of Heat and Mass Transfer, Vol. 34, No. 8, pp. 2133-2147

[19] Goodro, M., Park, J., Ligrani, P., Fox, M., and Moon, H.-K, 2008. "Effects of hole spacing on spatially-resolved jet array impingement heat transfer", *Int. J. Heat Mass Transfer*, Vol. 51, Nos. 25–26, pp. 6243–6253.

[20] Uysal, U., Li, P., Chyu, M.K. and Cunha, F.J., 2006, "Heat Transfer on Internal Surfaces of a Duct Subjected to Impingement of a Jet Array with Varying Jet Hole-Size and Spacing", Journal of Turbomachinery, Vol. 128, pp. 158-165

[21] Huang, Y., Ekkad, S.V., and Han, J.C, 1996. "Detailed Heat Transfer Coefficient Distributions Under an Array of Inclined Impinging Jets Using a Transient Liquid Crystal Technique." 9th International Symposium on Transport Phenomena in Thermal Fluids Engineering (ISTP-9), Singapore, June 25-28

[22] El-Gabry, L.A and Kaminski, D.A., 2004, "Experimental Investigation of Local Heat Transfer Distribution on Smooth and Roughened Surfaces Under an Array of Angled Impinging Jets." Journal of Turbomachinery, Vol.127, No. 3, pp. 532

[23] Sping, S., Xing, Y., and Weigand, B., 2012, " An Experimental and Numerical Study of Heat Transfer from Arrays of Impinging Jets with Surface Ribs", Journal of Heat Transfer, Vol. 134, 082201-1 – 082201-11

[24] Trabold, T.A. and Obot, N.T., 1987, “Impingement Heat Transfer within Arrays of Circular Jets Part II: Effects of Crossflow in the Presence of Roughness Elements”, Proceedings of the Internal Gas Turbine & Aeroengine Congress & Exhibition, May 31-June 4, Anaheim, California, 87-GT-200

[25] Andrews, G., Abdul Hussain, R., and Mkpadi, M., 2003, “Enhanced Impingement Heat Transfer: Comparison of Co-Flow and Cross-Flow With Rib Turbulators,” Proceedings of IGTC2003, Paper No. IGTC2003 Tokyo TS-075.

[26] Annerfeldt, M., Persson, L., and Torisson, T., 2001, “Experimental Investigation of Impingement Cooling With Turbulators or Surface Enlarging Elements,” Proceedings of ASME Turbo Expo 2001, New Orleans, LA, Jun. 4–7, Paper No. 2001-GT-0149.

[27] Chang, H., Zhang, D., and Huang, T., 1997, “Impingement Heat Transfer From Rib Roughened Surface Within Arrays of Circular Jet: The Effect of the Relative Position of the Jet Hole to the Ribs,” Proceedings of the International Gas Turbine and Aeroengine Congress and Exhibition, Orlando, FL, Jun. 2–5, Paper No. 97-GT-331.

[28] Chang, H., Zhang, J., and Huang, T., 1998, “Experimental Investigation on Impingement Heat Transfer From Rib Roughened Surface Within Arrays of Circular Jet: Effect of Geometric Parameters,” Proceedings of the International Gas Turbine and Aeroengine Congress and Exhibition, Stockholm, Sweden, Jun. 2–5, Paper No. 98-GT-208.

[29] Chang, H., Zhang, J., and Huang, T., 2000, “Experimental Investigation on Impingement Heat Transfer From Rib Roughened Surface Within Arrays of Circular Jets: Correlation,” Proceedings of ASME Turbo Expo 2000, Munich, Germany, May 8–11, Paper No. 2000-GT-220.

[30] Ekkad, S. V., Esposito, E. I., Kim, Y. W., 2012, “Zero-Cross-Flow Impingement via an Array of Differing Length, Extended Ports”, United States Patent, Number US 8,127,553 B2.

[31] Lee, C.S., Shih, T. I-P., Bryden, K.M., Ames, R. and Dennis, R.A., 2012, “Flow and Heat Transfer in a Jet-Impingement Configuration with no Cross Flows about Impinging Jets”, ASME Turbo Expo, GT2012-70080.

[32] Zu, Y. Q., Yan, Y. Y., and Maltson, J. D., 2009, “CFD Prediction for Multi-Jet Impingement Heat Transfer, ASME Turbo Expo, GT2009-59488.

[33] Thielen, L., Hanjalic, K., Jonker, H. and Manceau, R., 2005, “Predictions of Flow and Heat Transfer in Multiple Impinging Jet with an Elliptic-Blending Second-Moment Closure”,Internationa Journal of Heat and Mass Transfer, Vol. 48, No. 8, pp 1583-98.

[34] Rao, G. A., Kitron-Belinkov, M. and Levy, Y., 2009, Numerical Analysis of a Multiple Jet Impingement System, ASME Turbo Expo, GT2009-59719.

[35] Chen, S.P., Li, P.W., and Chyu, M.K., 2006, “Heat Transfer in a Airfoil Trailing Edge Configuration with Shaped Pedestals Mounted Internal Cooling Channel and Pressure Side Cutback,” ASME Turbo Expo, GT2006-91019.

[36] Chyu, M.K., Ding, H., Downs, J.P., and Soechting, F.O., 1998, “Determination of Local Heat Transfer Coefficient Based on Bulk Mean Temperature Using a Transient Liquid Crystal Techniques”, Experimental Thermal and Fluid Science, 18, pp. 142-149.

[37] Kline, S.J. and McClintock, F.A., “Describing Uncertainties in Single Sample Experiments,” Eng. (Am. Soc. Mech. Eng.), 75, pp. 3-8.

[38] Miller, N., Siw, S.C., Chyu, M.K. and Alvin, M.A., 2013. “Optimization of Single Row Jet Impingement Array by Varyin Flow Rates.”, Proceedings of ASME Summer Heat Transfer Conference, HT2013-17342, July 14-19

[39] Striegl, S.A. and Diller, T.E., 1984, “An Analysis of the Effect of Entrainment Temperature on Jet Impingement Heat Transfer,” ASME Trans. Journal of Heat Transfer, 106(4), pp 804-810

[40] Lamont, J.A, Ekkad, S.V., and Alvin, M.A., 2012, “Effects of Rotation on Heat transfer for a Single Row Jet Impingement Array with Crossflow,” ASME Trans. Journal of Heat Transfer, 134(8), pp 082202-1-082202-12